

**ACQUISITION AND RECONSTRUCTION OF BRAIN TISSUE USING KNIFE-  
EDGE SCANNING MICROSCOPY**

A Thesis

by

DAVID MATTHEW MAYERICH

Submitted to the Office of Graduate Studies of  
Texas A&M University  
in partial fulfillment of the requirements for the degree of

MASTER OF SCIENCE

December 2003

Major Subject: Computer Science

**ACQUISITION AND RECONSTRUCTION OF BRAIN TISSUE USING KNIFE-  
EDGE SCANNING MICROSCOPY**

A Thesis

by

DAVID MATTHEW MAYERICH

Submitted to Texas A&M University  
in partial fulfillment of the requirements  
for the degree of

MASTER OF SCIENCE

Approved as to style and content by:

---

John Keyser  
(Chair of Committee)

---

Andreas Klappenecker  
(Member)

---

Ergun Akleman  
(Member)

---

Valerie Taylor  
(Head of Department)

December 2003

Major Subject: Computer Science

**ABSTRACT**

Acquisition and Reconstruction of Brain Tissue Using Knife-Edge  
Scanning Microscopy. (December 2003)

David Matthew Mayerich, B.S., Southwestern Oklahoma State University

Chair of Advisory Committee: Dr. John Keyser

A fast method for gathering large-scale data sets through the serial sectioning of brain tissue is described. These data sets are retrieved using knife-edge scanning microscopy, a new technique developed in the Brain Networks Laboratory at Texas A&M University. This technique allows the imaging of tissue as it is cut by an ultramicrotome.

In this thesis the development of a knife-edge scanner is discussed as well as the scanning techniques used to retrieve high-resolution data sets. Problems in knife-edge scanning microscopy, such as illumination, knife chatter, and focusing are discussed. Techniques are also shown to reduce these problems so that serial sections of tissue can be sampled at resolutions that are high enough to allow reconstruction of neurons at the cellular level.

## **ACKNOWLEDGMENTS**

I would like to thank John Keyser and Bruce McCormick for introducing me to this project and for their patience and guidance throughout my research. I would also like to thank the National Science Foundation and the Texas Higher Education Coordinating Board who helped to fund this work. Finally, I would like to thank my family and friends, especially my mother and brother, Rosemary and Michael, who have always pushed for the best.

## TABLE OF CONTENTS

	Page
ABSTRACT.....	iii
ACKNOWLEDGMENTS.....	iv
TABLE OF CONTENTS.....	v
LIST OF FIGURES.....	vii
 CHAPTER	
I INTRODUCTION .....	1
A. Motivation .....	2
B. Main Results .....	3
II PREVIOUS WORK .....	4
A. Data Acquisition.....	4
B. Reconstruction .....	5
III KNIFE-EDGE SCANNING MICROSCOPE DEVELOPMENT .....	7
A. Introduction .....	7
B. Stage and Motion Control.....	8
C. Specimen Tank and Specimen Mounting.....	9
D. Collimator-Knife Assembly .....	10
E. Illumination Subsystem .....	11
F. Microscope and Camera Assembly.....	12
G. Image Acquisition Hardware and Software .....	13
H. Ribbon Extraction.....	14
IV DATA ACQUISITION.....	15
A. Tissue Preparation .....	15
B. Line Scanning .....	17

CHAPTER	Page
C. Tissue Sectioning.....	20
V ISSUES IN KNIFE-EDGE SCANNING .....	24
A. Knife Chatter and Abatement.....	24
B. Focusing Issues.....	28
C. Illumination Issues.....	31
VI IMAGE PROCESSING AND RECONSTRUCTION .....	35
A. Background Noise Removal.....	35
B. L-Block Reconstruction.....	38
VII RESULTS .....	40
A. Scanning of Golgi Stained Tissue and Alignment .....	40
B. Scanning and Reconstruction of Nissl Stained Tissue .....	43
VIII SUMMARY AND FUTURE WORK.....	46
A. Summary .....	46
B. Future Work.....	47
C. Conclusion .....	49
REFERENCES.....	50
APPENDIX A RECONSTRUCTION OF TISSUE SCANNED USING CONFOCAL MICROSCOPY .....	55
APPENDIX B KESM USER INTERFACE .....	58
VITA .....	67

## LIST OF FIGURES

	Page
Fig. 1. Knife-Edge Scanning Microscope image. ....	8
Fig. 2. Specimen mounting diagram (left) and specimen bed (right).....	10
Fig. 3. Laser refraction through the diamond knife.....	12
Fig. 4. Time Delayed Integration is used to increase the exposure of pixels. As the sample passes under an individual photon receptor, the light intensity value is summed and passed to the next register. The final output pixel is the sum of the light intensity received by all TDI registers for a single sampled point.....	18
Fig. 5. Volumetric data set construction. ....	21
Fig. 6. Stair-step sectioning.....	22
Fig. 7. Position error plot of the Z-axis stage. ....	25
Fig. 8. Knife chatter on specimen surface. ....	27
Fig. 9. Microscope focusing through binoculars (left) and with the imaging system (right).....	30
Fig. 10. Laser (left) and incoherent (right) illumination patterns on the knife surface. ...	33
Fig. 11. KESM images before (top) and after (bottom) noise removal and homogenization. ....	36
Fig. 12. Thionine stained mouse cortex before (top) and after (bottom) contrast enhancement.....	37
Fig. 13. Golgi stained mouse cortex before (left) and after (right) contrast enhancement. ....	37
Fig. 14. L-Block connectivity (left) and sample L-Block covering of Golgi stained mouse brain (right) [15]. ....	39
Fig. 15. Images of sequential sections of mouse brain at 10X (axial sectioning). ....	40
Fig. 16. Images of several neurons and their processes. ....	41

	Page
Fig. 17. Orthogonal sections of Golgi tissue visualized in Amira (left) and neuron processes reconstructed using L-Blocks (right). .....	42
Fig. 18. Nissl stained mouse brain at 10X (coronal section).....	43
Fig. 19. Close up of the lateral ventricle at 10X. ....	43
Fig. 20. Close up of the hippocampus at 10X. ....	44
Fig. 21. Isosurface reconstruction of the hippocampus (left) and density changes through the brain (right) using Amira. ....	44
Fig. 22. Reconstructions of a 0.15mm thick data set (left) and a portion of the hippocampus (right). ....	45
Fig. 23. Sequential confocal slices of GFP stained mouse brain at 60X.....	56
Fig. 24. Isosurface reconstruction of processes from confocal scans. ....	57
Fig. 25. Login Module.....	61
Fig. 26. Main Menu Module. ....	62
Fig. 27. Experiment Parameters Module.....	63
Fig. 28. Sectioning and Image Capture module. ....	64
Fig. 29. Module Flow of Control diagram. ....	65
Fig. 30. Interface Module / Database Interactions [27].....	66



## CHAPTER I

### INTRODUCTION

The imaging of the small animal brain at a cellular level of detail is an emergent technology, which promises to elucidate mammalian brain anatomy in unprecedented detail, revealing the density, morphology, and interconnectivity of neurons in the small animal. A new instrument of recent invention, the *Knife-Edge Scanning Microscope (KESM)*, makes possible three-dimensional microscopy of large biological specimens, for example, an entire mouse brain, at a cellular level of detail. The instrument has been designed to volume digitize a specimen (e.g., a plastic-embedded tissue block) at a maximum sampling resolution of 250nm in the image plane at rates up to 200Mvoxels/s. Depth resolution in this case is typically 500nm. The speed of the instrument is such that, potentially, an entire mouse brain (~1 cubic cm) can be scanned in one month of one-shift operation, yielding an uncompressed volume dataset of 26 terabytes.

This thesis addresses two critical issues in whole brain imaging of the mouse:

**Goal 1. Acquire scanned cortical tissue at a sufficient resolution and alignment to allow the reconstruction of cell bodies and their dendrites.** Minimal conditions for this cellular reconstruction are (1) serial sectioning and concurrent scanning of

---

This thesis follows the style and format of *IEEE Transactions on Visualization and Computer Graphics*

Golgi and Nissl stained mouse brain tissue at  $1.5\mu\text{m}$  resolution; (2) alignment of images through the stack of serial images (as demonstrated with Golgi-stained tissue). I describe a method for volume data acquisition from mouse cortical tissue at the proper resolution. I also demonstrate sufficient alignment using Golgi stained mouse brain.

**Goal 2. Demonstrate the reconstruction of Nissl stained mouse cortex.** After demonstrating proper alignment and resolution, I discuss how this data set is processed and reconstructed into a 3D model of cell bodies in the mouse brain.

Artifacts still significantly mar these preliminary studies as we struggle to tame the very demanding new technology required for imaging the entire mouse brain. The current limitations of knife-edge scanning microscopy are discussed.

## **A. Motivation**

The reconstruction of a complete neurological forest has many possible applications, both in neuroscience and computational neurobiology. Although we are capable of simulating interactions between small groups of neurons, our ability to study large areas of cortical tissue is still elusive because we lack sufficient information about the density, morphology, or interconnectivity of neurons in this tissue. Imaging large sections of cortical tissue promises to alleviate this lack of microstructure data.

In order to acquire these large data sets, techniques must be developed for the imaging of cortical tissue at a sufficient resolution to allow reconstruction. The development of a stable and fast method for gathering high-resolution, high-magnification images from sequential sections of cortical tissue is a major step in the research and study of cortical networks and how they work.

## **B. Main Results**

For this thesis I have completed the assembly of the Knife-Edge Scanning Microscope and developed the methods necessary to get large data sets from embedded tissues. This required developing and implementing processes for stage motion control, alignment, focusing, illumination, and image acquisition. I was able to retrieve high-resolution data sets from both Nissl and Golgi stained tissue to show the alignment and effectiveness of these techniques. Using these methods, I also show reconstructed cell bodies created from scanned volumetric data sets sampled from mouse tissue.

## CHAPTER II

### PREVIOUS WORK

#### A. Data Acquisition

Many methods exist for gathering high-resolution three-dimensional data sets from sampled tissue. One of the most common of these methods is confocal microscopy, which allows tissue to be imaged without sectioning [1, 2, 3, 4]. This method is generally used with fluorescent stains to create volumetric image stacks which can then be reconstructed as three-dimensional visualizations [5]. Although confocal microscopy provides high-resolution images, the scanning depth is limited to about 20-30nm since light scattering reduces the signal-to-noise ratio below a useful point.

Two-photon microscopy offers a solution to this problem [6, 7, 8] by only allowing light at the focal point within the specimen. Using two-photon microscopy, scanning depths can be approximately double those of confocal microscopy but are still limited due to light scattering. Achieving greater depths with either of these methods would require slicing the tissue into thin sections, which could then be scanned. This sectioning technique is time consuming and difficult to automate. The process also allows tissue warping to occur, making alignment between sections difficult [9].

Other methods have been developed which allow the ablation of scanned tissue on the surface using laser pulses [10]. This prevents tissue warping and eliminates the

need to embed or freeze tissue since there is no need to use a microtome to perform sectioning.

The techniques proposed in this thesis use a new method of image acquisition known as Knife-Edge Scanning Microscopy (KESM). KESM is a new technology that is being developed at the Department of Computer Science, Texas A&M University. With knife-edge scanning, an ultramicrotome uses a diamond knife to section tissue at the desired thickness while concurrently imaging the sectioned tissue. This allows for fast image acquisition of embedded tissue and an essentially unlimited scanning depth, since the tissue is removed during the imaging process.

## **B. Reconstruction**

A broad base of work exists in the areas of three dimensional reconstruction and image processing. Three-dimensional data sets can be visualized using *marching-cubes* or other isosurface generation algorithms [11, 12]. Other reconstruction methods such as volumetric ray tracing can also be used to visualize reconstructed tissue.

Although these methods work well for low-resolution MRI data and high-resolution cell bodies, these methods can be inefficient for entire neurons with many intertwined dendritic and axonal *processes*. Brent Burton researched the tracing of the stringy structure of neuronal processes across images gathered from sectioned tissue [13, 14]. This method allows the reconstruction of processes that span sections and also come close to other cell bodies and their processes.

McCormick, et al., also proposed a method of compressing and storing fine dendritic and axonal processes using an L-Block structure [15]. This structure minimizes the amount of space required to store high-resolution volumetric data sets by removing empty space from the images and storing only data corresponding to cells and their processes. This data is stored as a series of interconnected blocks, making it efficient for the compression of stringy structures such as neuronal processes. The L-Block structure also divides the space of the data set in a way that makes it conducive to the use of other volumetric visualization methods such as marching-cubes and volumetric ray tracing. This method is used in the reconstruction of neurons from KESM scans and will be discussed in more detail later (Chapter III).

## CHAPTER III

### KNIFE-EDGE SCANNING MICROSCOPE DEVELOPMENT

#### A. Introduction

The Knife-Edge Scanning Microscope (Fig. 1) was designed and developed by Bruce McCormick [16] at Texas A&M University. It is the first method thus far allowing the concurrent microscopic imaging of tissue while it is being sectioned. This allows us to gather large data sets at high resolution and magnifications in a relatively short time, while maintaining three-dimensional alignment of the volume data set. Since, at the time of this writing, the only KESM in existence is the unit constructed at Texas A&M University, all specific references to the KESM will refer to the unit in the Brain Networks Laboratory, Department of Computer Science, Texas A&M University.

The design of the KESM allows sections as thin as  $0.5\mu\text{m}$  thick to be cut from embedded tissue. The device itself consists of a mechanical stage, specimen tank, collimator-knife assembly, illumination subsystem, microscope, and image acquisition subsystem. The device allows the sectioning of embedded tissue using a diamond knife. As the tissue is cut, the slice is scanned through the microscope and processed by a cluster of five Dell servers.

## B. Stage and Motion Control

The motion of the tissue block under the stationary diamond knife is controlled by a series of mechanical and air-bearing stages. The stage assembly consists of three separate stages, which give the tissue block three degrees of movement. The X-axis stage allows smooth movement in the cutting direction, perpendicular to the edge of the knife. The Y-axis stage allows translation along the direction of the knife-edge, and the Z-axis stage is a vertical lift stage that supports the specimen tank and tissue.

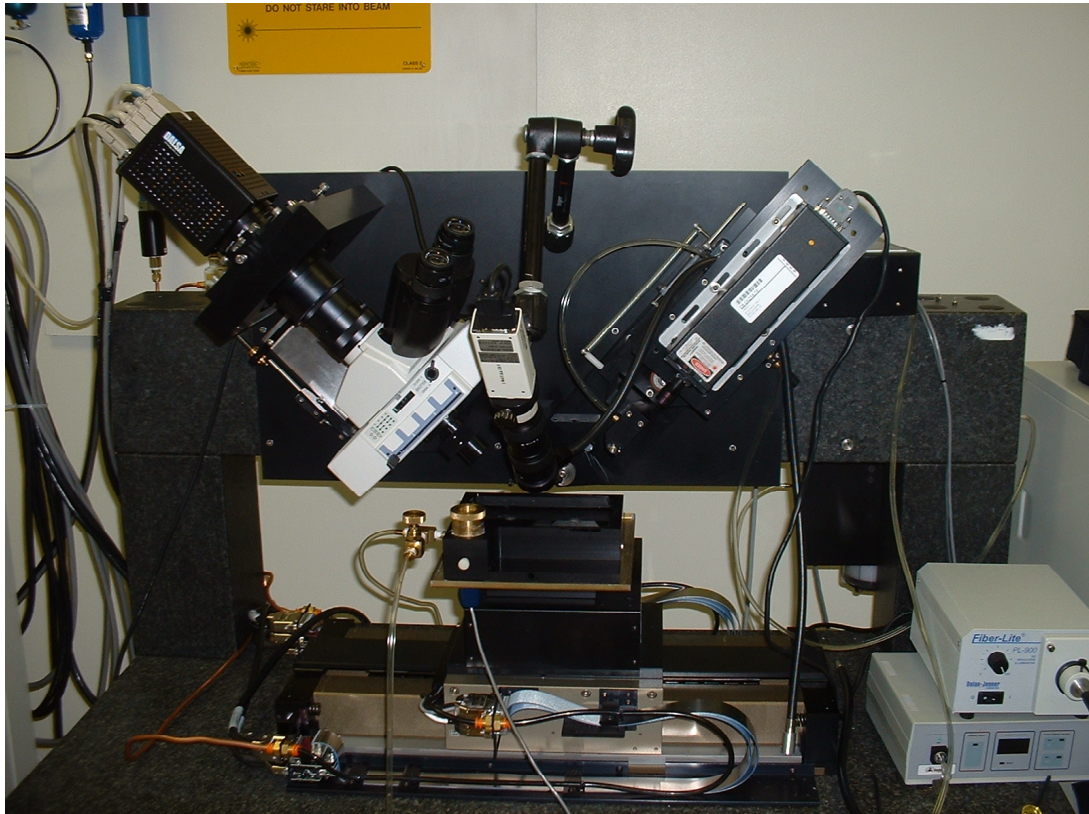


**Fig. 1. Knife-Edge Scanning Microscope image.**



At the time of these experiments, the KESM is using three custom-mounted Aerotech stages. The X-axis stage is a linear air-bearing unit that allows smooth cutting motion perpendicular to the knife-edge. The X-axis system is capable of maintaining a constant velocity up to 21mm/sec. The Y-axis stage is a linear mechanical stage. Unlike the air-bearing units, which are constantly seeking to maintain accuracy, the mechanical Y-axis stage tends to stick due to friction, maintaining a stable position for straight cutting. The Z-axis stage is a vertical lift stage that is primarily mechanical but uses air pressure to give support strength to the unit. The Z-axis stage allows us to make stable, straight cuts and is capable of supporting the weight of the specimen tank and mounted specimen. The positions of the X- and Y-stages are encoded within 20nm increments, while the Z-axis stage is encoded to 25nm. Servo resolution is typically +/- 3 encoder counts. For stability, the entire stage assembly is mounted on top of a 2-ton granite base to reduce induced vibration that may be visible when cutting at high magnifications with moving mechanical components.

### **C. Specimen Tank and Specimen Mounting**

The tissue specimen itself sits in an open tank atop the three-axis stage in an open tank. The tissue specimen is initially potted in a firm plastic polymer and molded into a keyed ring. This ring fits firmly into the specimen tank where it prevents the rotation of the tissue block (Fig. 2). Tightening a screw against the base of the ring further restricts movement of the sample ring.

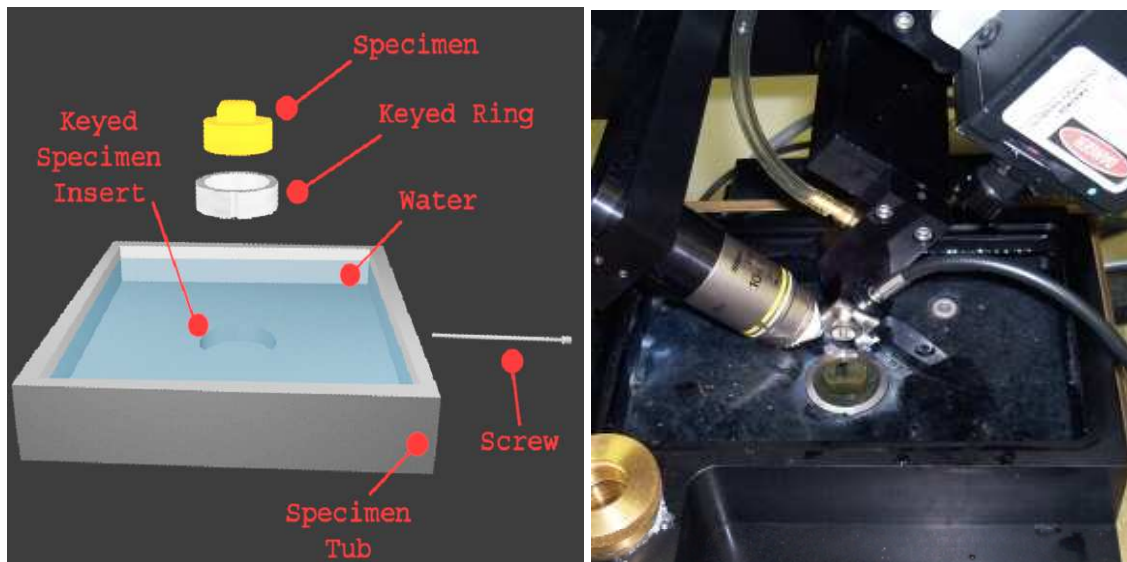


**Fig. 2. Specimen mounting diagram (left) and specimen bed (right).**

The tank is then filled with distilled water and the specimen block is submerged. The distilled water is used in conjunction with water-immersion microscope objectives. The higher index of refraction of the water allows objectives a higher numerical aperture, enabling tissue to be sampled at higher magnification. The specimen tank design could be extended so that oil immersion objectives could be used if we wish to sample tissue at magnifications greater than 40X.

#### **D. Collimator-Knife Assembly**

The Collimator-Knife Assembly (Fig. 1) consists of a removable diamond knife mounted onto a heavy, movable stage at 45° to the vertical. The stage provides the necessary weight behind the knife that is required for cutting but allows the knife to be retracted when necessary, allowing the user to manipulate the tissue sample. The collimator assembly is adjustable, allowing rotation around two axes as well as knife

retraction using a micrometer for fine adjustment. The Collimator-Knife Assembly is bolted to a massive granite bridge over the stage, which in turn is bolted to the granite slab supporting the stage.

For tissue sectioning, we use two different knife sizes. These are suited to the degree of magnification desired. In our initial system, these are 10X and 40X. When using the 10X objective we use a 5mm diamond knife. A smaller 1.2mm knife is used when imaging with the 40X objective. The field of view of the objective allows us to image roughly half of the knife width (e.g., 2.5mm with the 10X). We build the knives twice as wide as minimally necessary to reduce sharpening costs. As one half of the knife becomes dull, we can continue sectioning with the other half.

#### **E. Illumination Subsystem**

The Illumination Subsystem is mounted onto the Collimator Assembly stage and consists of an interchangeable laser and line generator optics. In our current system we have three lasers available: two 20mW lasers pumping at 473nm and 488nm and one 50mW laser pumping at 532nm. These frequencies were selected as the optimal for the excitation of florescent stains. The mounted laser beam is focused through a line generation lens and directed into the back of the diamond knife. The high incident angle at which the beam hits the back surface of the knife allows the light to enter the diamond (Fig. 3). The beam is then reflected off of the bottom of the laser and again refracted out of the top edge of the diamond knife. This projects the line onto the surface of the upper edge of the knife where it can provide illumination for sectioned tissue.

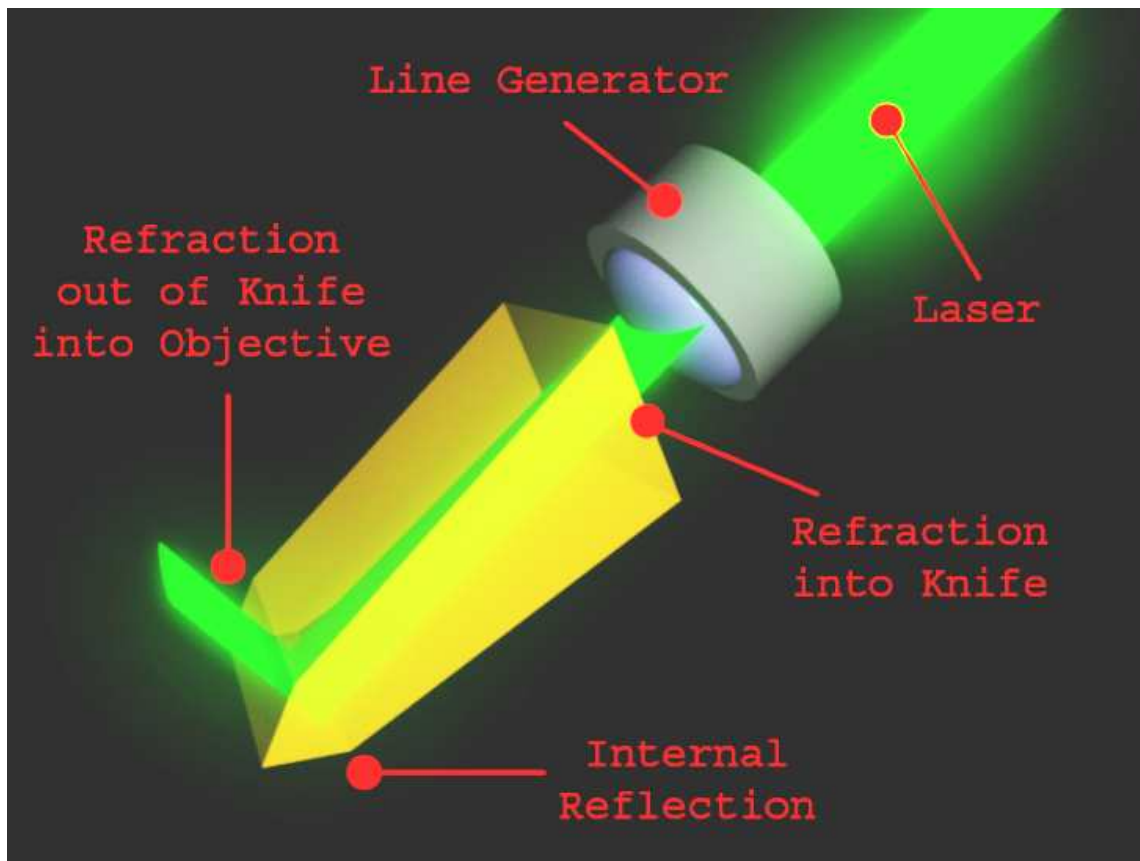


Fig. 3. Laser refraction through the diamond knife.

#### F. Microscope and Camera Assembly

The Image Acquisition Assembly consists of a Nikon microscope with replaceable objectives as well as two removable Dalsa line-scan cameras. We have 2X, 4X, 10X, and 40X objectives available for use with the microscope but primarily use the 10X and 40X objectives for higher-magnification imaging, allowing us to view neuron cell bodies and their processes.

The edge of the knife is viewed by the desired objective and the light is focused through the optical unit to be imaged by a high-sensitivity line scan camera. The image

is then reconstructed line-by-line as the stage moves the tissue sample across the edge of the knife. We have two Dalsa cameras for line-scan imaging. The monochrome camera has a line scan resolution of 4096 pixels and images at 44 kHz. The Dalsa color camera has half that resolution (2048 pixels) and also runs at a reduced speed of 28 kHz. These cameras, in combination with the 10X or 40X objective, allow the resolutions listed below (Table I).

TABLE I  
SAMPLING RATES FOR LINE SCAN CAMERAS

	DALSA 4096 Monochrome CT-F3-4096	DALSA 2048 Color CL-T7-2048
10X Nikon Objective	$\approx 0.6\mu\text{m} / \text{pixel}$	$\approx 1.2\mu\text{m} / \text{pixel}$
40X Nikon Objective	$\approx 0.3\mu\text{m} / \text{pixel}$	$\approx 0.3\mu\text{m} / \text{pixel}$

### G. Image Acquisition Hardware and Software

In order to maintain the highest possible bandwidth for image scanning, specific hardware is devoted to image acquisition. The high-sensitivity cameras send data directly to a camera server. The camera server at this time is a dual processor Intel Pentium III. Data from the camera is stored directly into one gigabyte of available memory through two EPIX camera control boards. The twin EPIX PIXCI D2X boards work concurrently to supply data from the camera into the server's main memory. Each card is responsible for the capture and storage of half of the scanned image (2048 pixels/cycle). In order to achieve maximum bandwidth, each card is installed on a separate PCI bus and is capable of 132MB/sec data transfers.

The EPIX board controls firing of the DALSA camera by either an internal clock or an outside TTL signal. In our case, the TTL signal is sent from the Aerotech stage and the camera firing is keyed to the position of the X-axis cutting stage.

The control software designed to work with the EPIX PIXCI cards are used for preliminary image processing (formatting) and storage. The XCLIB and PXIPL C libraries are used to format the images as TIFF files and store them on disk. These libraries also allow the update of database entries to keep track of stored image files for later processing [17]. Using the PIXCI software also provides the option of performing additional image processing such as compression and noise removal.

## **H. Ribbon Extraction**

In order to keep the cutting environment clean during sectioning, the tissue samples must be removed during sectioning. In order to accomplish this, we have installed a water circulation system that pulls water from the specimen tank through an outlet just above the knife and supplies filtered water back to the tank via an inlet in the base. In addition to keeping the specimen tank clean, the circulation pump prevents previously cut slices from interfering with imaging and helps to keep slices flat as they move along the top face of the knife while they are being cut.

## CHAPTER IV

### DATA ACQUISITION

#### A. Tissue Preparation

We have found that standard tissue staining procedures work well for KESM scanning, although special precautions and lengthy intervals must be taken to allow the stain to infiltrate an entire brain. Staining the entire mouse brain with Golgi was done by first saturating the brain with osmium-dichromate and then dyeing the cells by keeping the tissue in a silver nitrate solution. The complete Golgi staining process for an entire brain takes about two months.

Golgi has several advantages over other staining solutions since it reveals the entire neuron structure and only stains about one percent of the neurons in the tissue. These qualities were excellent for testing alignment of the KESM and Golgi stained tissue was therefore used as our initial scanning material. The disadvantage to Golgi staining, however, is that random cells are stained and its effects are therefore not reproducible.

For the Nissl stained tissue, the whole brain specimens were dyed with thionine. Thionine stains the RNA in the cytoplasm of all neurons as well as the DNA in all cell bodies. With Nissl staining, all cell bodies are visible but the dendritic arbors and axons remain unstained. With Nissl stains, we can reconstruct the distribution of all cell bodies

in the mouse brain, and in particular their distribution within the six layers of the cerebral cortex.

The Golgi tissue used in these experiments was stained and embedded by Dr. Roland Giolli in the School of Medicine at UC Irvine. The thionine Nissl tissue was stained and potted by Dr. Louise Abbott at the Department of Veterinary Anatomy and Public Health, College of Veterinary Medicine, Texas A&M University. Both samples were embedded in Poly/Bed 812 Resin, available from Polysciences, Inc. The tissue is prepared with Nadic Methyl Anhydride, also available in a kit with instructions from Polysciences. The alcohol wash eliminates any fluid in the brain tissue, which was then replaced by the 812 Resin and hardened in a Teflon mold. The embedding process takes about two days to complete and, once removed from the mold, the tissue is ready for sectioning.

Other embedding compounds can be used, although little experimentation with different compounds has been done using the KESM. When using microtomes, harder materials tend to provide better results. Plastics offer another possibility, although there has been little research done on how plastics affect the staining process. We are currently considering ways to increase the hardness of the specimen block through cooling. This process is common in cryo-microtomy and there are many cryo-microtomes available commercially (See Microstar Technologies).



## **B. Line Scanning**

Tissue slices are scanned into coherent images using a high-resolution and high-sensitivity line-scan camera. A 4096-pixel long, single pixel wide line is imaged along the leading edge of the knife. Our primary camera of choice is a DALSA CT-F3 High-Speed TDI Line Scan Camera. In order to get a high sensitivity at the speed at which we want to cut, the monochrome camera uses Time Delay Integration (described below) to remove artifacts from the generated pixels. The camera's output is a line 4096 pixels long and one pixel wide. The actual sensor in the camera consists of 4096x96 TDI registers.

Time Delay Integration is used to create a higher contrast image by increasing the amount of light received by the camera without any detriment to the imaging speed. The camera fires when it receives a digital signal from the stage. During one cycle, the camera completes two tasks. First of all, each TDI register receives an intensity value from its associated photon receptor. This value is added to the value currently stored in the register. Next, the register passes its currently stored value to the next register. The last TDI register outputs its value as the current pixel value (Fig. 4).

The firing command is sent to the camera by the stage controller. The controller is programmed to fire based on the position of the X-axis stage, as read out from its encoder. This firing position is dependent on the type of objective being used since the same tissue must be imaged under consecutive TDI photon receptors for a sharp image.

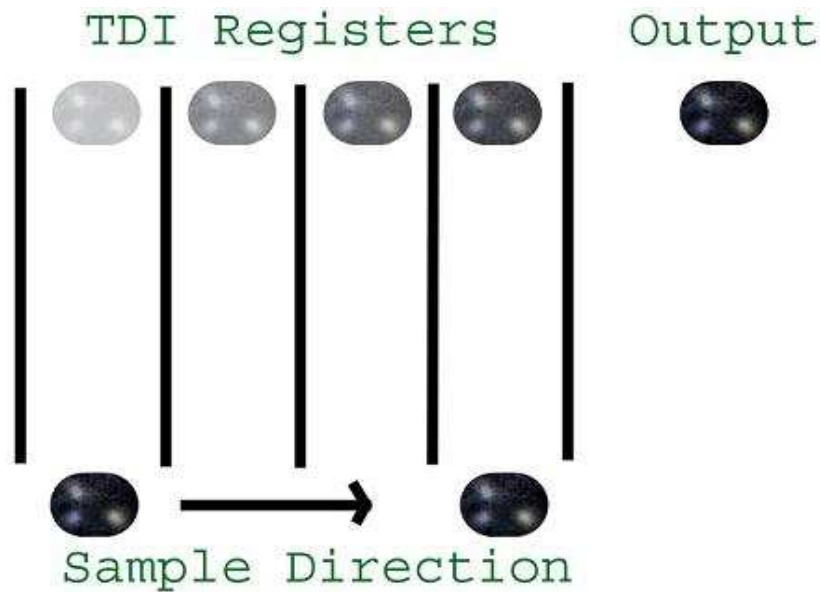


**Fig. 4.** Time Delayed Integration is used to increase the exposure of pixels. As the sample passes under an individual photon receptor, the light intensity value is summed and passed to the next register. The final output pixel is the sum of the light intensity received by all TDI registers for a single sampled point.

In addition to creating a sharper image, this method keys camera firing to the position of the stage rather than to time. This allows us to sidestep velocity error, particularly when the cutting cycle begins and ends.

Using Time Delay Integration also makes the sharpness of the image independent of the speed at which the stage moves. Increasing the speed of the stage simply reduces the amount of light received by the camera. The limiting factor on the speed of our system is therefore the line-scan rate of the camera. The DALSA CT-F3 monochrome camera that we use for imaging Golgi tissue is capable of running at 44kHz, ideally giving us a maximum cutting velocity of 26.4mm/sec using the 10X objective, and 6.6mm/sec (with the 40X objective). In practice, however, the limiting factor is based on the bus speed of the computer hosting the camera control board. This limits us to

approximately 28 kHz giving us a maximum cutting speed of 17mm/sec at 10X and 4.2mm/sec at 40X.

Although Time Delay Integration gives a sharper image, the increased number of registers creates a wider *footprint* on the edge of the knife. The aperture for the DALSA CT-F3 is 53.3mm x 1.3mm, where photoreceptors for each TDI register are 13.5 $\mu$ m wide. The 53.3mm-long line projects to the length of the knife-edge in the microscope. This line projects to approximately 2.5mm with the 10X objective and 0.625mm using the 40X objective. The 1.3mm width of 96 TDI registers projects to about 61 $\mu$ m on the surface of the knife using the 10X objective and 15.2 $\mu$ m with the 40X objective. Since the 10X objective was primarily used in these preliminary experiments, the camera is imaging a rectangle about 2.5mm long and 61 $\mu$ m wide. In order for the tissue to be properly imaged, it must be coherent across the knife-edge for approximately 61 $\mu$ m. If there were any change in tissue velocity or coherence in the 61 micron imaging zone, the camera output would appear blurred.

Keeping the ribbon coherent is a constant problem inherent in the knife-edge scanning technique, but I have found that there are several methods to reduce the problem. The water circulation pump and ribbon extraction system help to keep the ribbon moving along the surface of the knife by providing a constant water flow over edge of the knife. This circulation helps to prevent tissue sticking and movement contrary to the cutting direction.

The design of the DALSA camera also allows for the reduction of the number of TDI registers used in the integration process. For the CT-F3 camera, I was able to

reduce the number of active TDI registers to 32. This reduces the amount of light available to the camera three-fold but also reduces the imaged region to about  $20.3\mu\text{m}$  (for the 10X objective). These methods allowed me to get sharp section images and can be further refined for higher quality images. At higher magnifications image coherence becomes easier since the illuminated width being imaged is inversely proportional to the magnification. In fact, increasing the number of TDI registers at higher magnifications could improve the image quality by allowing significantly more light into the camera.

### **C. Tissue Sectioning**

The sectioning process uses a stair-stepping method that reduces wear on the diamond knife and allows for faster, more accurate reconstruction of the scanned tissue. When a single slice is taken, the entire slice is stored in the system as a sequence of square images. In the case of the monochrome camera, these images are  $4096 \times 4096$  pixels (Fig. 5). After several slices are taken, the images can be stacked on top of one another to create a series of blocks. These blocks are typically 50 – 100 images deep and a large part of the 3D reconstruction can be done on them independently.

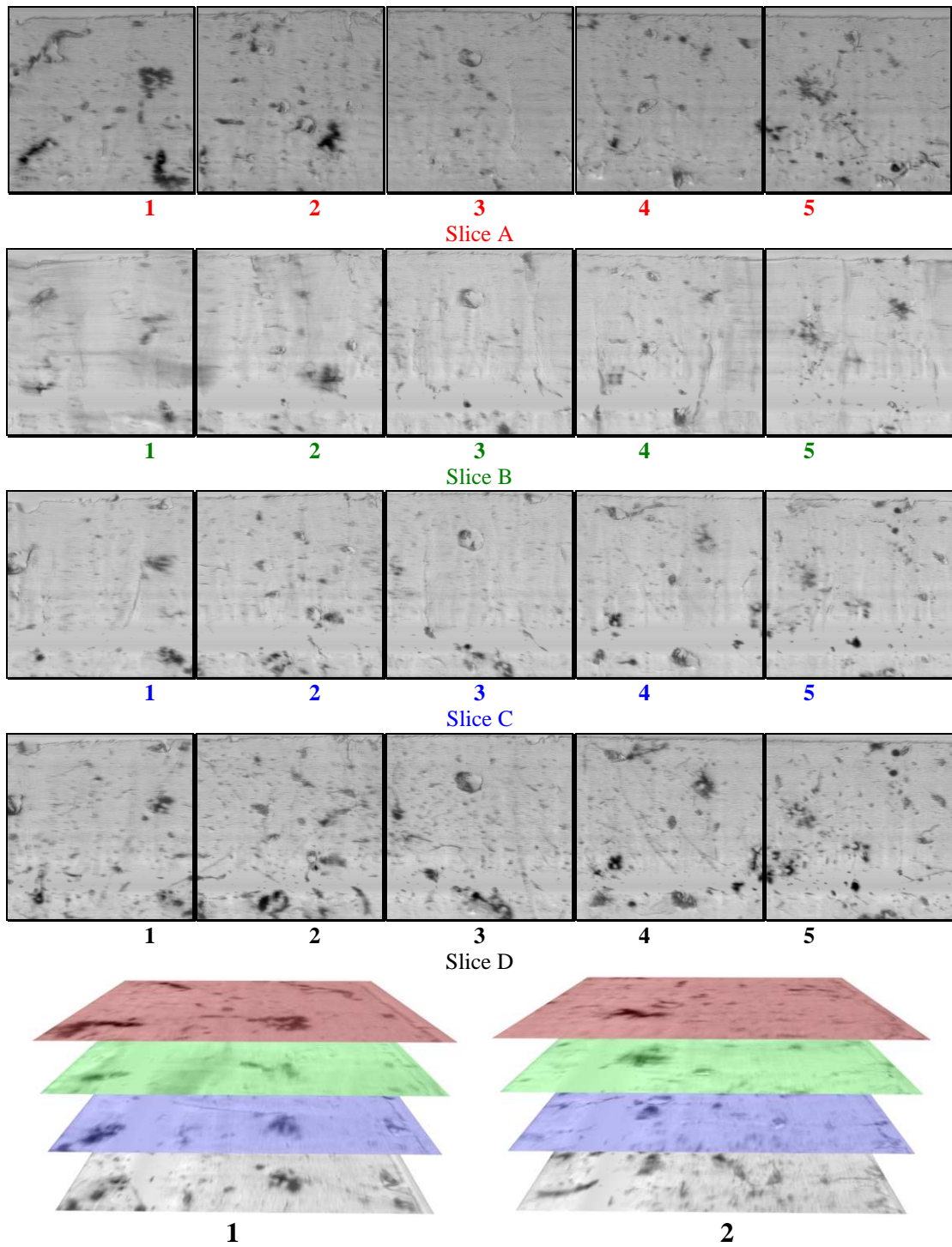
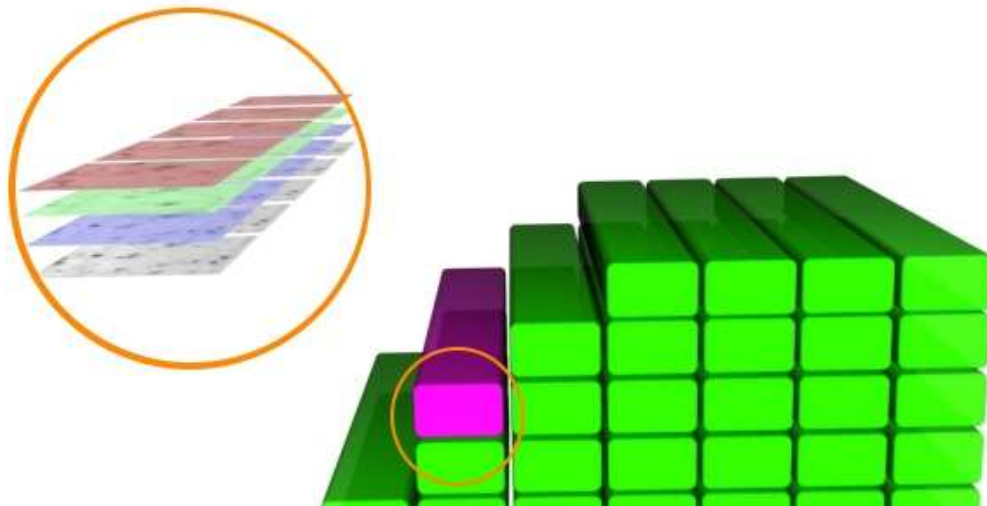


Fig. 5. Volumetric data set construction.

As cutting progresses through the specimen, block sequences are cut at discrete intervals along the Y and Z-axes [18]. These blocks create a staircase shape in the tissue (Fig. 6). The tissue is scanned like this for several reasons. First, this allows us to use half of the knife at a time, reducing wear on the knife-edge. Cutting in this way prevents the rest of the knife-edge from prematurely dragging along uncut tissue. Preventing knife contact with uncut tissue also reduces knife chatter that is otherwise prevalent in the system and greatly reduces the quality of the image.



**Fig. 6. Stair-step sectioning.**

Scanning of the tissue, as indicated above, is performed with a high-speed Dalsa line-scan camera. The camera is aligned with the light coming off of the edge of the diamond knife. As the stage moves the tissue block under the knife, the camera records pixel data from the slice that is being cut. The stage motion controller controls the firing of the camera. Depending on the objective and camera we are using, the stage is pre-programmed to fire at set increments along the X-axis. A rough estimate of the required

firing rate can be computed; however the system must be fine-tuned to compensate for inaccuracies in the power of the objective.

## CHAPTER V

### ISSUES IN KNIFE-EDGE SCANNING

#### A. Knife Chatter and Chatter Abatement

One of the biggest challenges in ultramicrotome development is hardware stability. At high magnifications very small vibrations become visible, making stable imaging difficult. During knife-edge scanning this problem becomes even more complex since each slice must be as complete and uniform in thickness as possible. In order to obtain the best possible image, this uniformity must be maintained through the imaging process, allowing all TDI registers to receive light from the same points on the moving tissue ribbon.

The major cause of noise in the system is knife chatter. Knife chatter is defined as undesirable movement of the knife as it skips across the tissue surface. Although the hardest type of chatter to remove is periodic, random vibrations in the KESM do contribute to the problem. Outside vibrations are reduced by making the KESM as stable as possible. Mounting the stage on a two-ton granite base reduces external vibrations.

Vibrations caused by servo seeking of the three stages can also introduce knife chatter. These are particularly true in the Z- axis stage since the X- axis stage is constantly moving in one direction while imaging and the Y-axis moves perpendicular to the chatter direction. Using a Z-axis mechanical stage reduces this source of chatter



since these stages have a tendency to stick due to friction between mechanical parts. The image below (Fig. 7) is a plot of the Z-axis position error at the end of a cut. Although the position accuracy is within 20nm when the stage is not in motion, the rapid velocity changes that occur as the X-axis changes direction can cause an error in the Z-axis position of over 8 $\mu$ m. Therefore, it is important to start X-axis motion well before knife contact with the tissue and end it well after. This helps to prevent major inaccuracies in stage position while cutting.

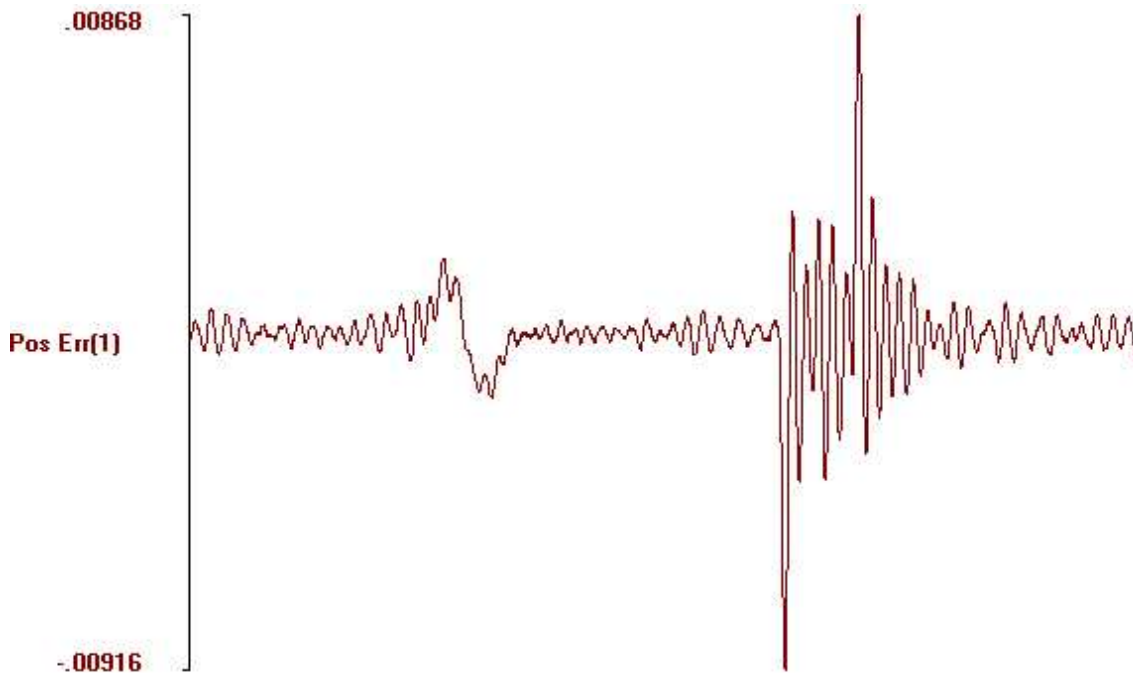


**Fig. 7. Position error plot of the Z-axis stage.**

Finally, the stability of the collimator-knife assembly is very important in sectioning. Microscopic movements in the knife positioning adjustments can cause the knife to move as pressure from the tissue block is pushed against it. Since knife position

adjustments were necessary for focusing as well as changing objectives, the knife position could not be completely static. It is also necessary for the knife to be retractable for tissue placement. In order to perform these adjustments micrometers and screws applied pressure to aluminum plates, allowing fine adjustments to the position and orientation to the diamond knife and collimator assembly. After finding that the aluminum allowed too much motion in the assembly, the KESM was refurbished using sapphire, rather than aluminum, plates. These allowed much more stable adjustments and reduced the vibration of the knife-collimator assembly.

I have found, however, that the primary cause of knife chatter is due to the compression of the tissue under the blade. This occurs when pressure applied by the knife causes the tissue to compress slightly at the knife tip [19, 20, 21, 22]. As cutting continues, this pressure increases and overcomes the weight holding the knife down. This causes the knife to jump slightly, introducing obvious noise into the image and creating a bump on the tissue surface. One precaution taken to reduce this compression is to use a hard plastic polymer as the embedding compound, making the tissue sample very stiff and resistant to compression (Ch. III). It is also important that the knife remains under heavy loading and offers firm resistance to the pressures caused by cutting. We cannot mount the blade rigidly, however, because this could cause damage to the knife in severe cases of tissue compression and limits the fine positioning of the blade.

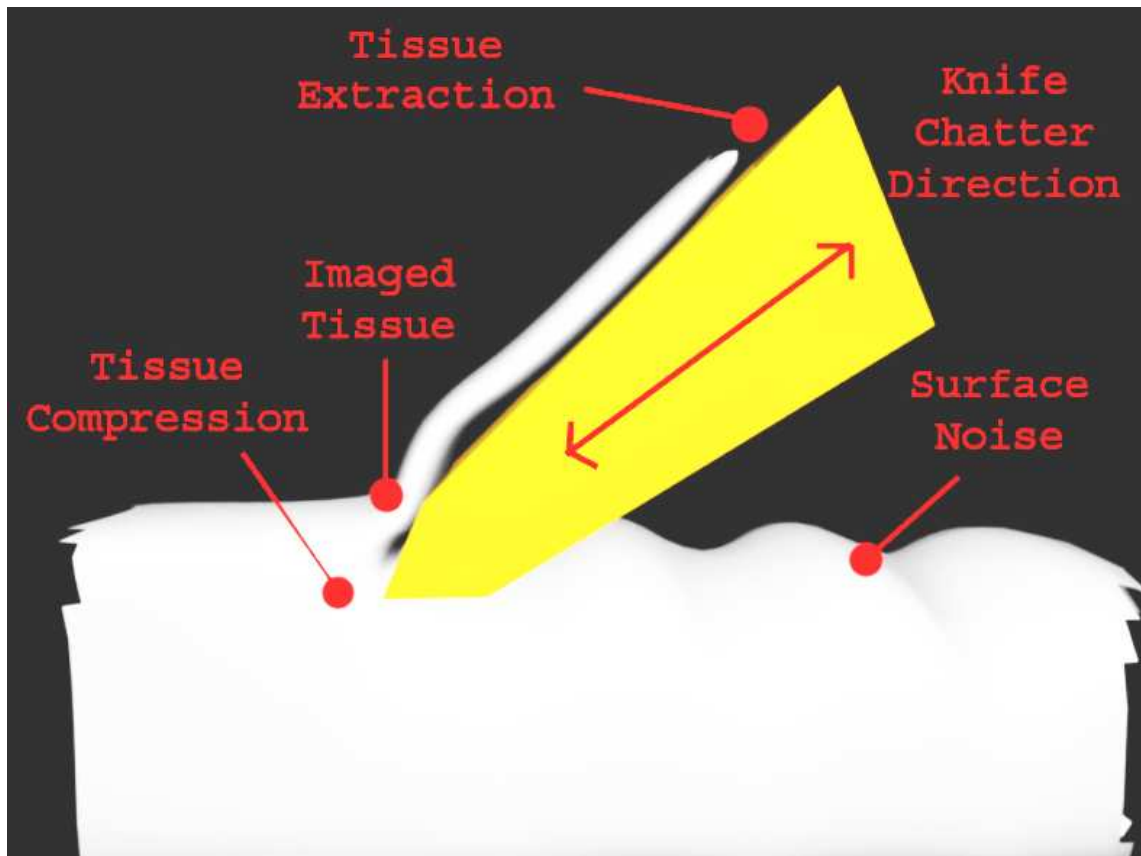


**Fig. 8. Knife chatter on specimen surface.**

Even with a rigid system and a choice of a hard potting compound, chatter seemed to get worse as sectioning continued. Over time, a sinusoidal (“wash board”) pattern develops on the surface of the embedding compound (Fig. 8). Over several consecutive slices, this sinusoidal pattern reinforces chatter in the current section. To deal with this chatter problem, I experimented with different cutting speeds. Slower speeds of around 5mm/sec produced high-frequency chatter on the tissue surface. Increasing the cutting speed caused lower-frequency chatter, however higher-frequency components began to appear between waves.

The solution to this reinforcement effect was to consistently change the frequency of the knife chatter by cutting sequential slices at different velocities. I found that a small change in velocity of about 20 percent gave significantly better results. This made the knife chatter much less regular and the tissue slices were cut in a more uniform thickness. The change in light intensity in the image can be easily compensated for since the amount of light received is inversely proportional to the velocity of the stage. The image brightness can be adjusted, as long as the velocity is recorded or a regular velocity-changing method is used.

## **B. Focusing Issues**

Obtaining a sharp image is important when creating a three-dimensional data set. In order for the image to contain as much data as possible, each pixel must provide an accurate sample of the focused light at its sample point. There are two major adjustments involved in focusing the KESM. Optical adjustment involves the proper positioning of the image acquisition hardware and objective. This positioning is dependent on the type and magnification of the objective being used and can be primarily performed visually through the microscope binoculars. Firing rate adjustment involves choosing the proper position increment at which the stage fires. Proper focusing ensures that the same tissue is under the proper photoreceptors for each TDI register.

## **B.1. Optical Focusing**

Adjusting the distance between the knife and objective focuses the microscope. This adjustment is made using a micrometer that directly adjusts the position of the objective. Increasing or decreasing the distance between the diamond knife and the objective moves the image plane, allowing the KESM user to fine-tune image focus. Since the microscope is always imaging moving tissue, however, there are several complications in obtaining the ideal image focus. First of all, viewing the knife-edge through the microscope binocular eyepiece and focusing on the edge of the diamond knife can achieve a general position for the objective. For the most part, this focusing can be done using the microscope objective focus adjustment (Fig. 9). Fine adjustments may require use of the camera, since individual pixels can be viewed. Using the camera, however, requires that a corner of the knife be visible in the image since the cutting edge is never actually visible. Since TDI integration does not occur along the Y-axis of the image, focusing on the corner of the knife is achieved by adjusting the objective position until a hard edge is visible in the image.

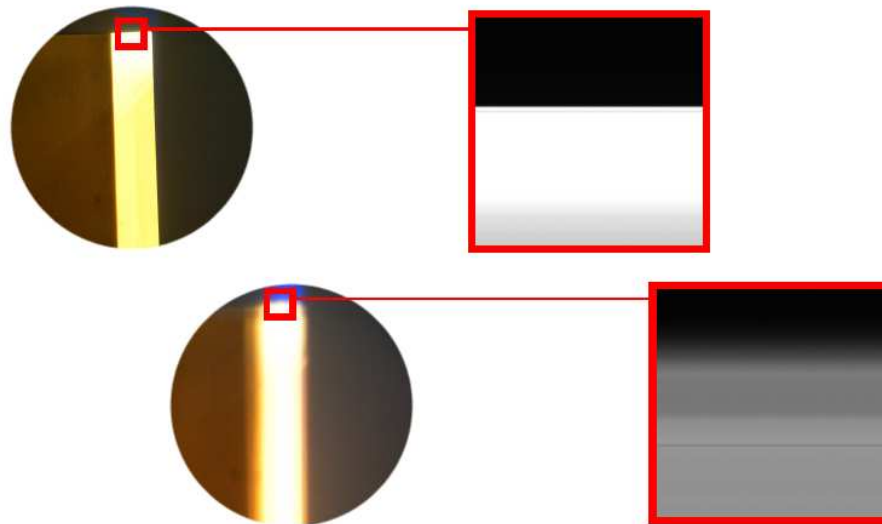


**Fig. 9. Microscope focusing through binoculars (left) and with the imaging system (right).**

Even after the knife-edge is in focus, additional adjustments may be required to compensate for the thickness of the tissue. This adjustment depends on the magnification being used and, specifically, on the width of the focal plane of the objective. Adjusting the focus to slightly above the knife-edge can correct for tissue thickness.

## **B.2. Firing Rate Adjustment**

Although Time Delay Integration and proper focusing can result in a sharper image, integrating out artifacts in lighting and environmental effects such as dust particles, it does cause some problems when being used at a high magnification. First of all, at 10X and higher levels of magnification, the focal width is very small and the objective must be adjusted to effectively focus on the tissue being scanned. Because the magnification must be manually adjusted, the amount of magnification has a small

amount of error. This error does not degrade the quality of the images or interfere with the results; however it does change the footprint of the TDI on the tissue surface. Basically, this changes the length of the pixel projected onto the tissue surface. If the magnification factor of the objective were exactly 10X, we would know to signal a TDI increment approximately every 0.6 $\mu$ m. However, since this is not the case, we have to dynamically adjust the firing rate of the camera. An improper adjustment results in blurring along the X-axis of the image.

In order to dynamically perform this adjustment, I had to allow changes in the firing rate within the user interface. However, the stage control card does not allow firing commands to be changed while a single stage move command is being executed. Therefore the firing rate had to be changed between consecutive serial sections. This adjustment is made by changing the size of the position increment at which the stage fires. For the most part, this focusing method relies on trial and error. The most effective method is to take a sequence of slices at different firing rates. Consecutive images can be stored in the frame buffer of the camera control server and compared for focus. For fine focusing detail, a Fast Fourier Transform can be performed on the image sequence. As the firing rate becomes more accurate, higher-frequency components become more visible in the image.

### **C. Illumination Issues**

The original KESM Illumination Subsystem was designed to take advantage of fluorescent stains, similar to those used in confocal or two-photon microscopy. As the

magnification and sampling rate increases, the light must be collimated properly to provide illumination for the camera. In the following sections, I will address diffraction problems with the original laser light model as well as problems when using an incoherent light source.

### **C.1. Laser Diffraction Patterns**

Although the original KESM design called for laser illumination through the diamond knife (Ch. III), interference patterns were visible on the surface of the knife, causing banding in the output image. In the bands visible in the output image, the falloff between light and dark pixels is very sharp, where many pixels were either saturated or totally absent of light. The banding was stable along the Y-axis and could be subtracted out, however the saturation or lack of light in many pixels results in a loss of data when scanning the tissue.

This banding problem turned out to be due to two components. First of all, speckle in the laser image, though not unexpected, was causing the surface of the knife to be illuminated irregularly. At a high magnification, laser speckle is not uncommon and one of the uses of the TDI camera system is to integrate out light irregularities. A line generation lens is used to focus the laser into a single line, which is to be aligned with the optics on the camera. Most of the speckle lies outside of the line and would therefore not be visible in the image. The problems with this proposed remedy were that the line was difficult to align with the camera and that refraction through the microscope optics frequently caused the line to bend, making the alignment process more difficult.



Proper focusing of the laser did not completely solve the banding problem because there is also a diffraction component that was obvious when looking at the surface of the knife. The dark and light bands visible on the knife surface are due to interference effects caused by the coherent laser light passing through the knife. I was unable to find a coherent line of light where this interference pattern did not occur; therefore the banding remained a problem. Since this is an effect of the knife geometry and the pattern is such a low spatial frequency, the TDI integration is not able to cancel out the interference patterns.

Allowing focused laser light to pass through a fiber optic cable before refracting into the knife eliminates interference patterns, but also decreases the intensity of the illumination. This allows us to scan fluorescent materials at magnifications of 10X, however scaling up the magnification will require more advanced methods for light collimation.

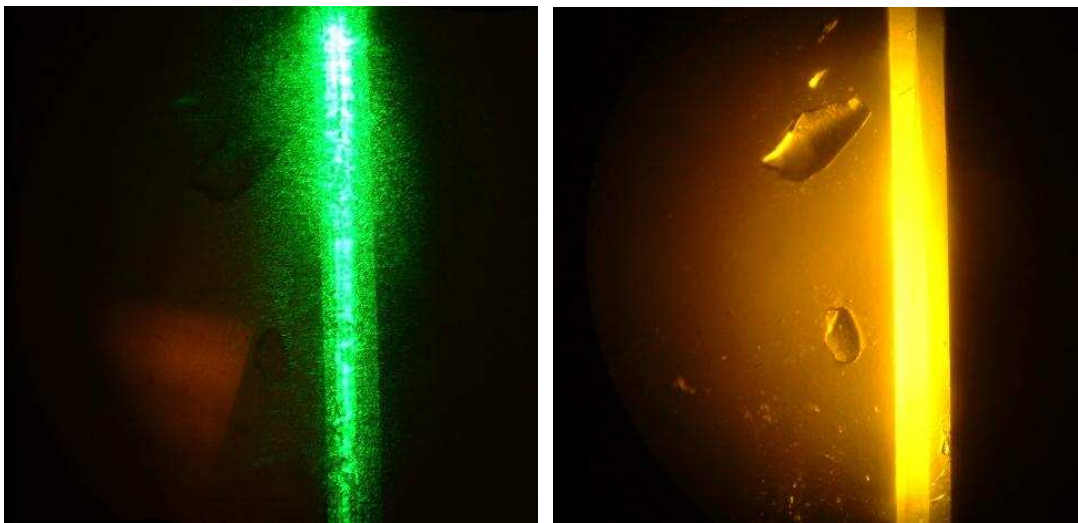


**Fig. 10. Laser (left) and incoherent (right) illumination patterns on the knife surface.**

## **C.2. Light Intensity**

For the results in this thesis, I used an incoherent fiber optic light source to illuminate the edge of the knife (Fig. 10). I have found that there are several advantages to this method when using non-fluorescent stains. First of all, incoherent light provides soft, even illumination across the surface of the knife. Incoherent white light also allows color imaging with the DALSA CL-T7.

The major advantage that coherent light provides is a high level of light intensity with relatively low power consumption and no need to change lamps. When using fiber optic illumination, light intensity quickly became a problem since coherent light is more difficult to collimate with our current design. Adapting the polished fiber-optic cable to the diamond knife allowed enough light to penetrate for 10X imaging. Imaging at 40X magnification is not possible with our current illumination system and will presumably be solved using a newly introduced Nikon fluorescence light source with liquid optic fiber terminated by collimation optics, allowing the light output through the diamond knife to be focused properly to provide light for our current objectives.

## CHAPTER VI

### IMAGE PROCESSING AND RECONSTRUCTION

After the desired data has been sampled from the embedded tissue, several artifacts must still be removed from the images for the datasets to be useful. Most of the operations we use are well-known image processing techniques. These include filters used in image homogenization and the removal of background noise. Contrast enhancement is also helpful for bringing out details in low-contrast stains such as thionine, used in Nissl staining. In addition, simple and adaptive thresholding methods are used to eliminate white-space data from the images for compression and visualization.

#### **A. Background Noise Removal**

Background noise occurs in the scanned images for a number of reasons. First of all, the knife itself is not perfect and certain artifacts and imperfections in the diamond knife can be seen in the images, although these are rare if the camera is aligned properly. Since we are using a TDI line-scan camera, knife artifacts will be consistent through all images since the knife doesn't move relative to the camera. Any artifact in the knife will appear as a discolored streak that is repeated through each image. These streaks can be removed simply by sampling the knife either before or after cutting. This gives a single

pixel line sample of the knife that can be subtracted from each row of the captured images to remove the noise.

One problem that can result from this method is a loss of data if any pixel is completely obstructed from receiving light. If any knife artifact is stopping a pixel from receiving light, the knife must be replaced or repaired to avoid data loss. This type of data loss is similar to the data loss experienced due to laser light diffraction patterns through the knife as described previously (Ch. V).

Any remaining knife chatter causes another form of background noise, which can be removed by homogenizing the image. Since this noise is very regular, sampling lines of pixels along both axes of the image and subtracting the mean tends to remove any remaining knife noise (Fig. 11).

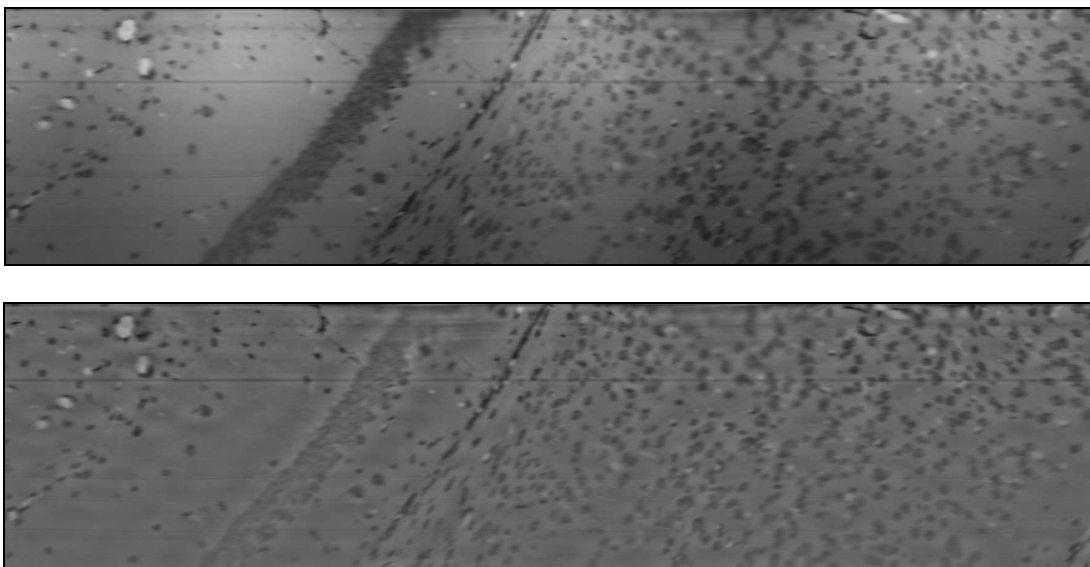


**Fig. 11. KESM images before (top) and after (bottom) noise removal and homogenization.**

In addition to noise removal, contrast enhancement may also be necessary for some low-contrast stains such as thionine for Nissl tissue (Fig. 12). Contrast enhancement can also be useful in higher-contrast stains like Golgi since it can bring out smaller details in cell processes, making reconstruction from layer to layer easier.

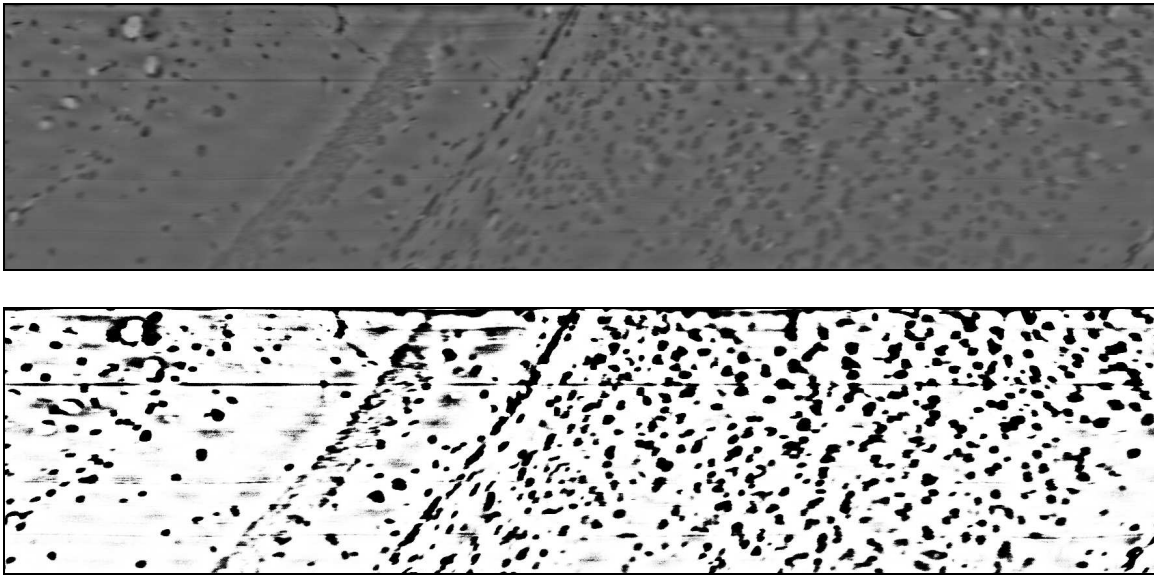


Fig. 12. Thionine stained mouse cortex before (top) and after (bottom) contrast enhancement.

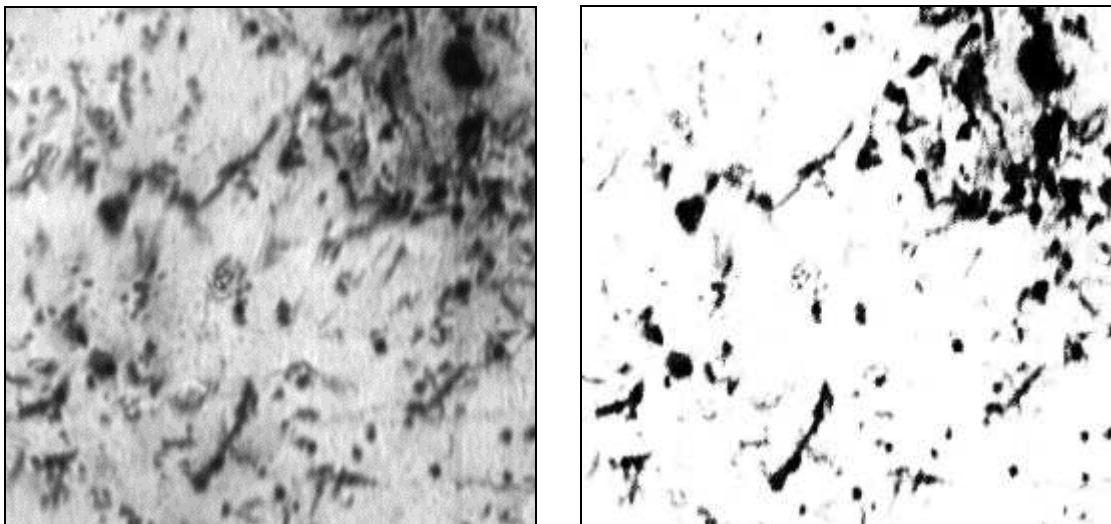


Fig. 13. Golgi stained mouse cortex before (left) and after (right) contrast enhancement.

## **B. L-Block Reconstruction**

The L-Block reconstruction method is an advanced compression scheme developed in the Brain Networks Laboratory by Bruce McCormick, et al. [15] and is designed to preserve connectivity data in sparse volumetric data sets. These data sets are similar to those created through Golgi or GFP staining where small percentages of entire neurons are stained. The shape of neuronal processes results in thin stringy structures throughout the data set as well as vast amounts of white-space data and background noise.

This reconstruction method is most useful with Golgi stained tissue and can be used to visualize neuronal processes running through the data set. Since these processes are extremely thin (often less than  $1\mu\text{m}$  in diameter) they provide a means of proving alignment of the Knife-Edge Scanning Microscope.

A basic L-Block covering is created first by establishing a reasonable threshold to exclude white space. A single block is assigned to each pixel that is not excluded by the threshold. Consecutive iterations eliminate smaller blocks and create larger blocks containing volumetric data. Neighboring blocks are linked together to preserve position data (Fig. 14). This dramatically reduces the amount of disk space required to store the data set since only the L-block positions, contents, and connectivity data are required for reconstruction of the data set.

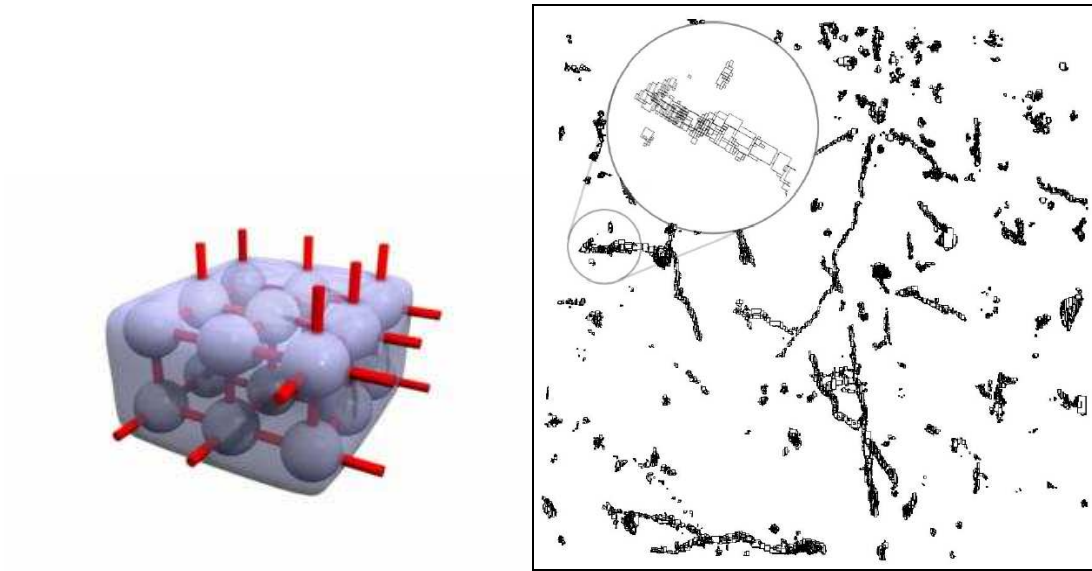


**Fig. 14. L-Block connectivity (left) and sample L-Block covering of Golgi stained mouse brain (right) [15].**

The L-Block technique also divides the three-dimensional space, making the data easy to traverse. This special subdivision can be utilized to simplify intersection detection for volumetric ray tracing and can assist in creating an isosurface from the stored data.

## CHAPTER VII

### RESULTS

#### A. Scanning of Golgi Stained Tissue and Alignment

Initial scans of 10X Golgi stained tissue were designed to test whether consecutive serial images had sufficient alignment for reconstruction. Since the Golgi staining process stains entire neurons, their dendrites provide convenient strands with which to test alignment. The images below are examples of unprocessed Golgi slices from the KESM (Fig. 15).

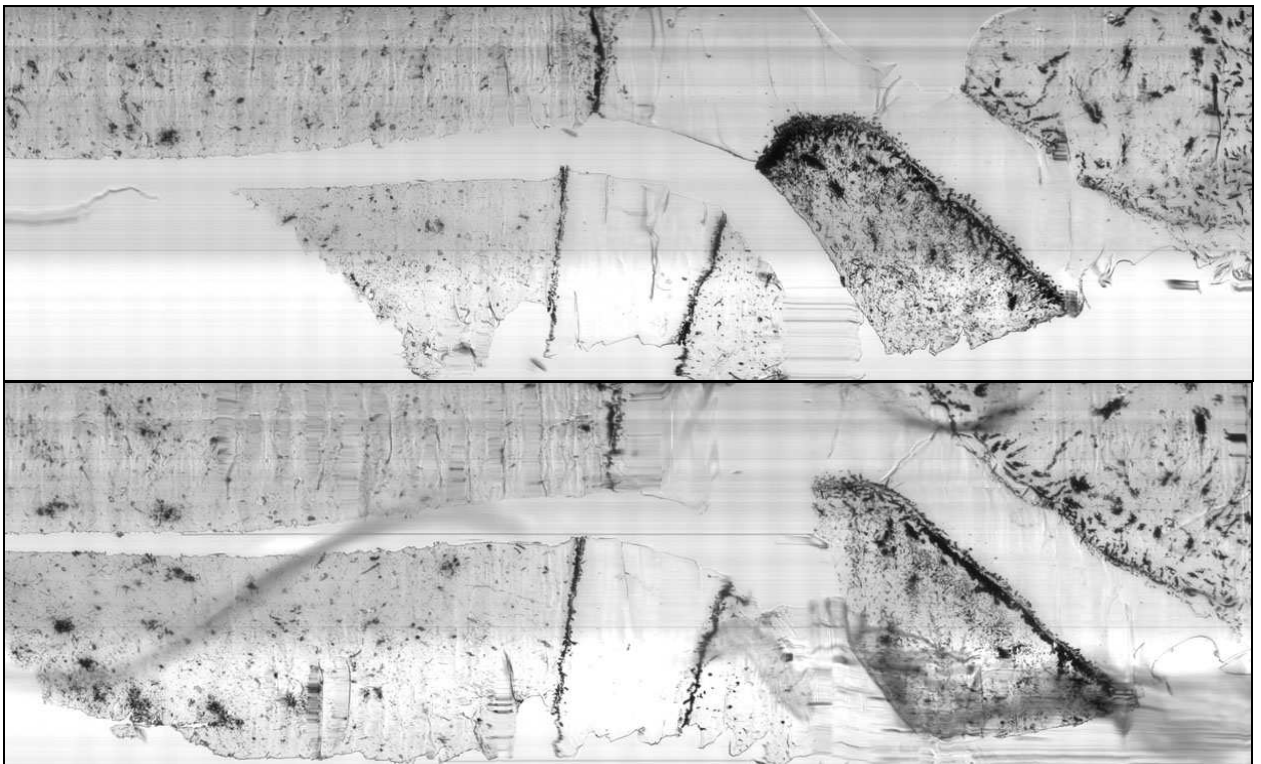


**Fig. 15. Images of sequential sections of mouse brain at 10X (axial sectioning).**



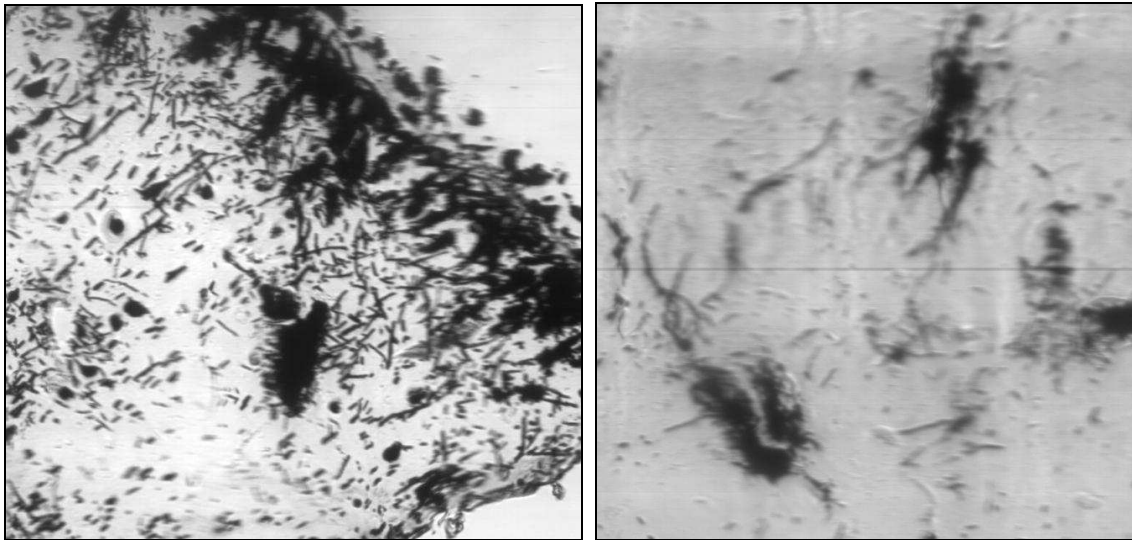


**Fig. 16. Images of several neurons and their processes.**

At magnifications of 10X, neuron cell bodies and segments of thick neuronal processes are clearly visible in individual slices. In order to show that the alignment of the KESM images is sufficient, a 3D data set was created and orthogonal slices taken, allowing us to view dendrites through the image stack.

Several of the reconstructions and visualizations below were created using Amira [23], a medical visualization and isosurface extraction toolset. As shown in the image above (Fig. 16), even without contrast and image enhancement, individual dendrites can be traced through the image stack along all three planes. As can be seen in most of the thicker segments, alignment is no more than a pixel off, approximately  $0.6\mu\text{m}$  in this case, from one slice to another. This is sufficient alignment to allow for reconstruction.

There are cases in scanning when areas of a slice are blurred or useless due to knife chatter or errors in ribbon extraction. As long as the KESM is exhibiting good

alignment, we can interpolate segments through bad slices. This also becomes necessary if processes become too thin to follow at the scanned magnification and resolution.

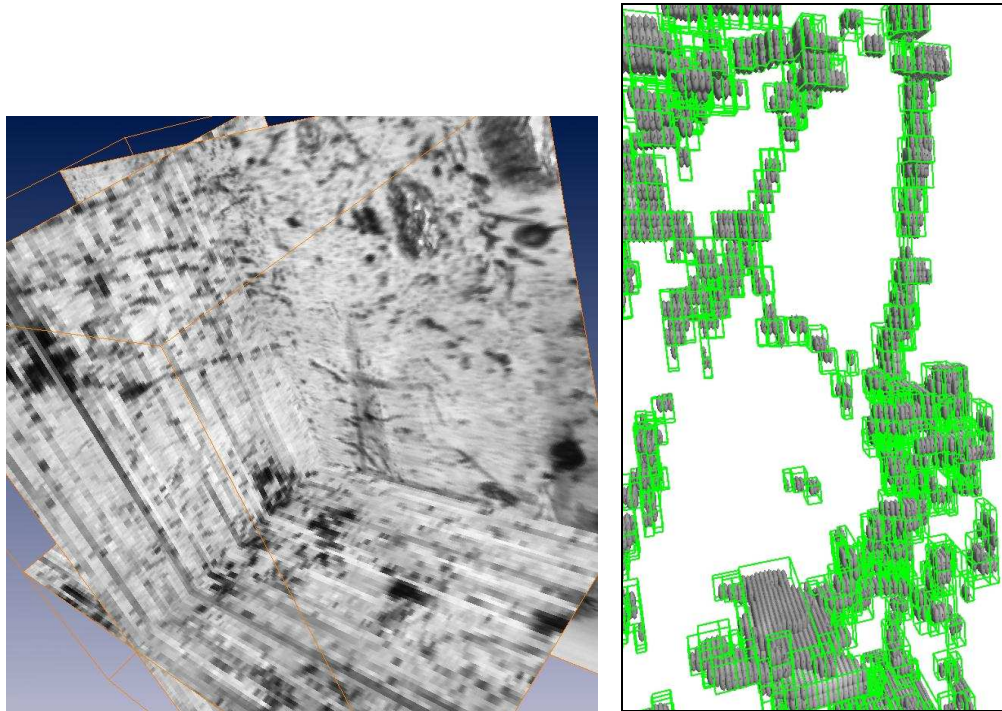


**Fig. 17. Orthogonal sections of Golgi tissue visualized in Amira (left) and neuron processes reconstructed using L-Blocks (right).**

The figure above (Fig. 17) shows that the L-Block reconstruction algorithm is able to find and compress the data set. Individual threads are visible and span the data set in all three dimensions, indicating that the KESM is producing images that are in alignment. The data stored in the L-Block covering can be used to more easily visualize the neurons or to extract connectivity data.

## **B. Scanning and Reconstruction of Nissl Stained Tissue**

The sectioning and reconstruction of Nissl stained tissue allows the testing and visualization of KESM alignment in dense structures. Since Nissl stain labels all cell bodies, the stain is used to visualize changes in cell density and within specific structures in the brain tissue. The images below are coronal slices of mouse brain. The slice (Fig. 18) shown below shows the lateral ventricle, hippocampus, and ventral part of the mouse cortex. Different layers of the mouse brain are clearly visible as density changes.

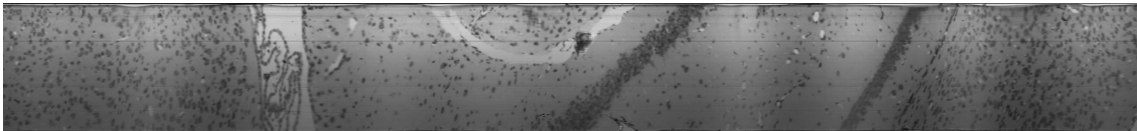


**Fig. 18. Nissl stained mouse brain at 10X (coronal section).**

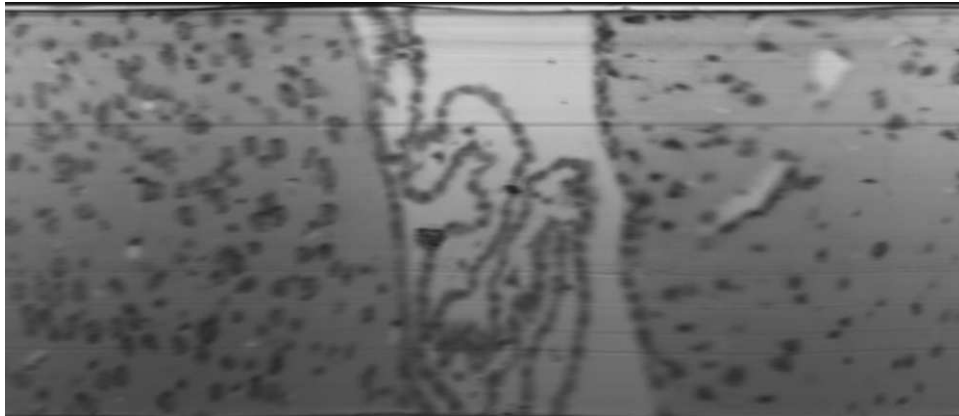


**Fig. 19. Close up of the lateral ventricle at 10X.**

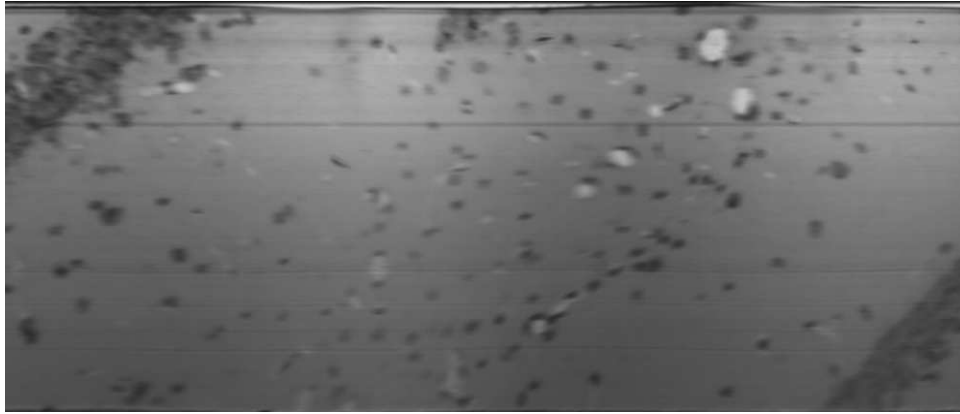


**Fig. 20. Close up of the hippocampus at 10X.**

The two images above (Fig. 19, 20) show closer images of both the lateral ventricle, running through the central area of the mouse brain and the hippocampus. At this magnification and resolution, the individual cells that outline the lateral ventricle can be seen.

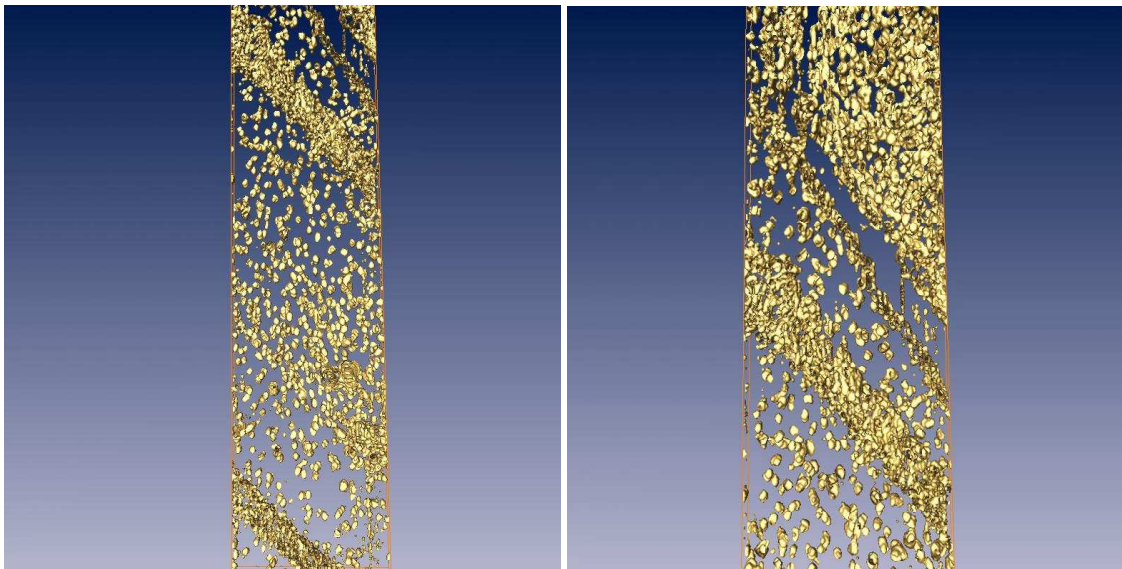


**Fig. 21. Isosurface reconstruction of the hippocampus (left) and density changes through the brain (right) using Amira.**

The images above (Fig. 21) show three-dimensional reconstructions of cell bodies above and within the hippocampus. This data set is gathered from tissue sections approximately  $1.5\mu\text{m}$  thick. The data for this reconstruction was gathered from single imaged plank 20 sections deep ( $\approx 0.03\text{mm}$ ). The visualizations below (Fig. 22) are from a larger data set  $\approx 0.15\text{mm}$  deep.

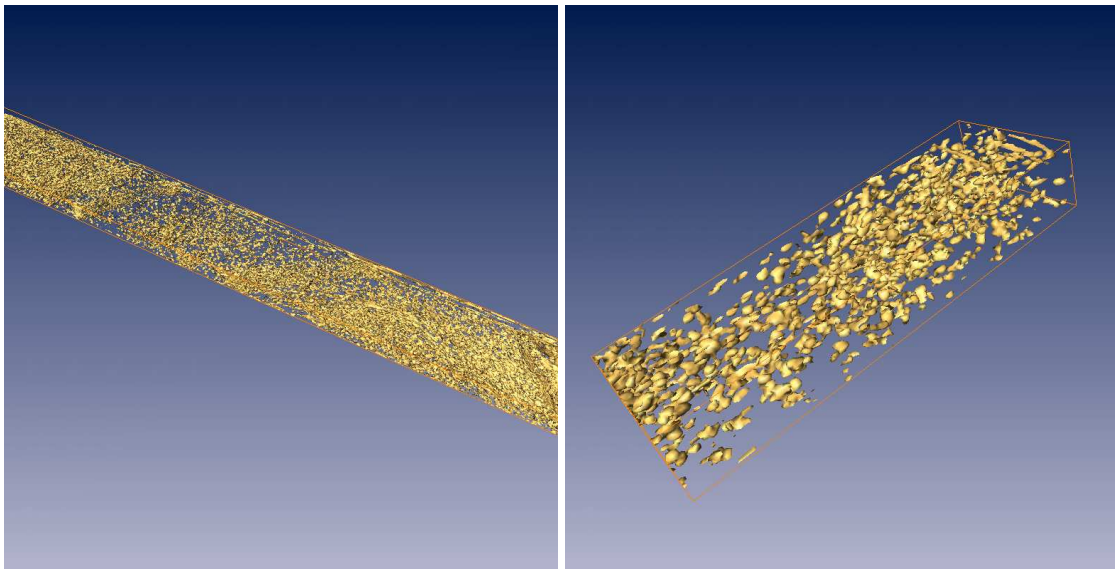


**Fig. 22. Reconstructions of a 0.15mm thick data set (left) and a portion of the hippocampus (right).**

## CHAPTER VIII

### SUMMARY AND FUTURE WORK

#### A. Summary

In this thesis I have shown the feasibility of gathering large data sets representing whole brain tissue scanned at a neuronal level of detail. These data sets allow for the three-dimensional reconstruction and visualization of neuron morphology.

I have described the design of the Knife-Edge Scanning Microscope that was used to gather these data sets and have discussed the overall alignment of the basic components required to operate the system. Several of the problems I have had in retrieving these initial data sets, including knife chatter, focusing, and light diffraction issues have been described above. I also outlined our immediate solutions to these problems and will propose future refinements, which will allow us to retrieve even higher quality data sets.

In addition to hardware issues, I have also discussed the details of our scanning algorithms used in our user interface design. Several of these algorithms, such as the stair-stepping method for sectioning, were found to be necessary to preserve volumetric alignment. Others, like the left and right sectioning methods used to prolong the life of the diamond knife, were convenient for minimizing knife sharpening.

After describing how the initial data sets were retrieved, I have covered the image processing strategy we use to refine these data sets. These include methods for

removing noise artifacts and dealing with any residual knife chatter. I also discussed instrument alignment issues and the problems inherent in tissue compression. Additionally, reconstruction methods I used to gather connectivity data and to visualize the results have been described. These methods include using isosurface reconstruction software, such as that from Amira as well as the L-Block reconstruction and compression method useful for “stringy” data sets created by intertwined dendrites.

Finally, I have shown and described data sets gathered from stained tissues. These data sets include cell body reconstruction from Nissl stained mouse brain tissue, as well as the reconstruction of neurons scanned from Golgi stained mouse brain. Finally, KESM microscopy (Appendix A) is compared to confocal scanning, another method for gathering similar data sets.

## **B. Future Work**

Some of the most obvious future developments to Knife-Edge Scanning are upgrades to our current KESM system. Most notably, greater stability in the Collimator-Knife Assembly could reduce knife chatter even more. Improved alignment and focusing adjustments would greatly improve the ease with which we can initialize the system. Also, there are higher intensity illuminators available that could be used, with appropriate collimating lenses, to increase the available light through the objective. This would lead to a reduced need for Time-Delay Integration beyond the current 32 registers used in the camera. A combination of reduced knife chatter and a thinner camera footprint could allow us to image thinner slices of tissue. The stage accuracy allows us

to cut slices below  $0.5\mu\text{m}$  however, due to chatter and tissue cohesion problems, these initial experiments were performed using slices 1-2 $\mu\text{m}$  thick.

Objectives of increased magnification would help to distinguish between individual neurons and identify synapses. This would give a much clearer picture of how neurons are interconnected. In order to obtain a usable numerical aperture for the objective, magnifications greater than 40X would best be achieved with oil immersion objectives. A redesign of the knife assembly and the ribbon removal system could allow for the use of oil immersion objectives and increase the possible resolution of the images.

There have also been significant advances in server bus speeds that could allow us to eliminate the server bottleneck at present restricting the speed at which tissue could be cut and scanned. EPIX also has new cameras available that store image data on board, allowing even higher frame-rates since image data can be sent to the server cluster during the knife's return stroke.

The Brain Networks Laboratory has also been working on using florescent stains with the KESM. This was the initial modification for the use of a laser as an illumination source. Due to the diffraction patterns, however, we will have to find a new method of using fluorescent stains. Fluorescent imaging plays a central role in reconstructing a complete brain network. The current transgenic stain we are working with, GAT1 – GFP transgenic mice, exhibits green fluorescent protein (GFP) and allows us to exclusively target all interneurons [24, 25]. Other types of neurons could be targeted as well, allowing a piecewise reconstruction of cortical networks. If



connectivity information were extracted, more accurate and advanced simulations could be run to explore the functionality of cortical networks [26].

### **C. Conclusion**

The research described in this thesis has created the groundwork for the acquisition and reconstruction of high-magnification data sets of neural tissue. I have shown that it is feasible to collect large data sets describing the topology and distribution of neurons at the microscopic level. I have described solutions to the common problems in the development and operation of an advanced microtome as well as problems particular to Knife-Edge Scanning Microscopy. The data sets collected for this research sample brain tissue at the neuronal level deeper than any other known form of modern microscopy. I have shown that knife-Edge Scanning Microscopy is a feasible method for the fast construction of data sets that represent brain tissue at a microscopic level. The KESM system is also not limited to thin samples of tissue like other microscopy techniques such as confocal and two-photon. Finally, I have also shown that images scanned using KESM are in registration and can be reconstructed and visualized using common volumetric techniques. In addition to visualization, these techniques can be used as a base for retrieving more detailed data sets describing the interconnectivity of neural networks.

## REFERENCES

- [1] T.R. Corle, G.S. Kino, *Confocal Scanning Optical Microscopy and Related Imaging Systems*. San Diego: Academic Press, 1996.
- [2] M. Gu, *Principles of Three Dimensional Imaging in Confocal Microscopes*. River Edge, NJ: World Scientific, 1996.
- [3] A. Kriete, *Visualization in Biomedical Microscopies*. New York: VCH, 1992.
- [4] C. Sheppard and D.M. Shotton, *Confocal Laser Scanning Microscopy*. Oxford: BIOS Scientific, 1997.
- [5] R. Dingledine, *Brain Slices*. New York: Plenum Press, 1984.
- [6] A.A. Eggert, R. van der Voort, R. Torensma, V. Moulin, O.C. Boerman, W.J. Oyen, C.J. Punt, H. Diepstra, A.J. de Boer, C.G. Figdor, G.J. Adema, "Analysis of dendritic cell trafficking using EGFP-transgenic mice", *Immunology Letters*, Vol. 89, no. 1, pp. 17-24, 2003.
- [7] C. Buehler, K.H. Kim, C.Y. Dong, B.R. Masters, and P.T.C. So, "Innovations in two-photon deep tissue microscopy", *IEEE Eng. Med. Biol. Mag.*, Vol. 18, pp. 23-30, 1999.
- [8] V.E. Centonze, and J.G. White, "Multiphoton excitation provides optical sections from deeper within scattering specimens than confocal imaging," *Biophys J.* Vol. 75, pp. 2015-2024, 1998.
- [9] W. Denk, J.H. Strickler, and W.W. Webb, "Two-photon laser scanning fluorescence microscopy," *Science* Vol. 248, pp. 73-76, 1990.

- [10] P.S. Tsai, B. Friedman, A.I. Ifarraguerri, B.D. Thompson, V. Lev-Ram, C.B. Schaffer, Q. Xiong, R.Y. Tsien, J.A. Squier, D. Kleinfeld, "All optical histology of brain tissue: Serial ablation and multiphoton imaging with femtosecond laser pulses," *Proceedings of CLEO*, 2003.
- [11] C. Barillot, B. Gibaud, J. Scarabin, and J. Coatreux, "3D Reconstruction of Cerebral Blood Vessels," *IEEE Computer Graphics and Applications*, Vol. 5 pp. 13-19, 1985.
- [12] J.K. Udupa, and D. Odhner, "Shell Rendering," *IEEE Computer Graphics and Applications*, Vol. 13 pp. 58-67, 1993.
- [13] B.P. Burton, "Automated 3D Reconstruction of Neuronal Structures from Serial Sections", M.S. Thesis, Department of Computer Science, Texas A&M University, College Station, 1999.
- [14] B.P. Burton, B.H. McCormick, R. Torp, and J.H. Fallon, "Three-dimensional reconstruction of neuronal forests", *Neurocomputing*, Vol. 38-40 pp. 1643-1650, 2001.
- [15] B.H. McCormick, B. Busse, Z. Melek and J. Keyser, "Polymerization Strategy for the Compression, Segmentation, and Modeling of Volumetric Data", Technical Report 2002-12-1, Department of Computer Science, Texas A&M University, College Station, December 2002.
- [16] B.H. McCormick, "Development of the Brain Tissue Scanner", Technical Report, Department of Computer Science, Texas A&M University, College Station, March 18, 2002.

- [17] W. Koh, “Distributed, Web-based Microstructure Database for Brain Tissue”, M.S. Thesis, Department of Computer Science, Texas A&M University, College Station, 2000.
- [18] W. Koh and B.H. McCormick, “Specifications for Volume Data Acquisition in Three-Dimensional Light Microscopy”, Technical Report TR2003-7-5, Department of Computer Science, Texas A&M University, College Station, 2003.
- [19] M. Davies and T. Burnes. “Thermomechanical Oscillations in Material Flow During High-Speed Machining”, *Phil. Trans. R. Soc. Lond. A.*, Vol. 359, pp. 821-846, 2001.
- [20] S. Gabor, “Modeling Nonlinear Regenerative Effects in Metal Cutting”, *Phil. Trans. R. Soc. Lond. A.*, Vol. 359, pp. 739-757, 2001.
- [21] F. Moon and T Kalmar-Nagy, “Nonlinear Models for Complex Dynamics in Cutting Materials”, *Phil. Trans. R. Soc. Lond. A.*, Vol 359, pp. 695-711, 2001.
- [22] M. Wiercigroch and E. Budak, “Sources of Nonlinearities, Chatter Generation and Suppression in Metal Cutting”, *Phil. Trans. R. Soc. Lond. A.*, Vol. 359, pp. 663-693, 2001.
- [23] Konrad-Zuse-Zentrum fur Informationstechnik Berlin and Indeed – Visual Concepts GmbH, *Amira – User’s Guide and Reference Manual*, Berlin, Germany, 2002.

- [24] C.S. Chiu, K. Jensen, I. Sokolova, D. Wang, M. Li, P. Deshpande, N. Davidson, I. Mody, M.W. Quick, S.R. Quake, H.A. Lester, “Number, density, and surface/cytoplasmic distribution of GABA transporters at presynaptic structures of knock-in mice carrying GABA transporter subtype 1-green fluorescent protein fusions”, *The Journal of Neuroscience*, Vol. 22 no. 23 pp. 10251-66, 2002.
- [25] L.M. Houdebine, et al., *Animal Transgenesis and Cloning*. Wiley Press, Hoboken, NJ, 2003.
- [26] J.M. Bower, and D. Beeman, *The Book of GENESIS: Exploring Realistic Neural Models with the General Neural Simulation System*, Springer Telos, Pasadena, CA, The Electronic Library of Science, 1998.
- [27] C.B. Stevens and D. Mayerich, “BTS User Interface”, Technical Report, Department of Computer Science, Texas A&M University, College Station, January 24, 2003.

### **Supplemental Sources Consulted**

- C. Ellis, Roy, *The microtome: function and design*, IMVS Division of Pathology, The Queen Elizabeth Hospital, Woodville, South Australia.
- J.C. Fiala, Three-Dimensional Structure of Synapses in the Brain and on the Web, *World Congress on Computational Intelligence*, Honolulu, HI, 2002.
- F. Joachim, M. Radermacher, P. Penczek, J. Zhu, Y. Li, M. Ladjadaj, A. Leith, SPIDER and WEB: Processing and Visualization of Images in 3D Electron Microscopy and Related Fields, *Journal of Structural Biology*, Vol. 116, pp. 190-199, 1996.

- J. Miao, K.O. Hodgson, D. Sayre, An Approach to three-dimensional structures of biomolecules by using single-molecule diffraction images, *Proceedings of the National Academy of Sciences*, Vol. 98, pp. 6641-6645, 2001.
- V.B. Mountcastle, *Perceptual Neuroscience: The Cerebral Cortex*, Harvard University Press, Cambridge, MA, 1998.
- J.V. Pelt, A. Dityatev, and H.B.M. Uylings, Natural Variability in the Number of Dendritic Segments: Model-Based Inferences About Branching During Neurite Outgrowth, *The Journal of Comparative Neurology*, Vol. 387, pp. 325-340, 1997.
- P.A. Penczek, R.A. Grassucci, F. Joachim, The ribosome at improved resolution: new techniques for merging and orientation refinement in 3D cryo-electron microscopy of biological particles, *Ultramicroscopy*, Vol. 53, pp. 251-270, 1994.
- P. Stern, and J. Marx (Editors), Special Review on Dendrites: Beautiful, Complex, and Diverse Specialists, *Science*, Vol 290, pp. 735-758, 2000.

## APPENDIX A

### RECONSTRUCTION OF TISSUE SCANNED USING CONFOCAL MICROSCOPY

#### A.1. Confocal Scanning of Green Fluorescent Protein

A recent development in staining techniques is the use of transgenic animals that exhibit fluorescence. Through the genetic manipulation of a parent animal, offspring can be made to exhibit fluorescent protein stains in selected neurons. Unlike Nissl, transgenic stains cause the entire cell body to fluoresce. Transgenic brain tissue also has a significant advantage over Golgi staining in that a single type of neuron can be targeted. This can allow the piecewise reconstruction of an entire cortical network by the selective staining of individual neuron types.

The ultimate goal of the Brain Networks Laboratory's KESM project is to create a brain atlas using transgenic mice as the preliminary subjects. For the initial experiments, we have mice available that are engineered to express Green Fluorescent Protein in GABAergic neurons (e.g., interneurons).

As an initial test of the effectiveness of fluorescence in the GAT1 – GFP mouse brain, a confocal microscope was used to take consecutive images every 0.5 $\mu$ m at 60x magnification. These images (Fig. 23) were taken without destroying the tissue, however as the microscope scans through the tissue block, light dispersion increases, reducing the ability to see small diameter neuronal processes.

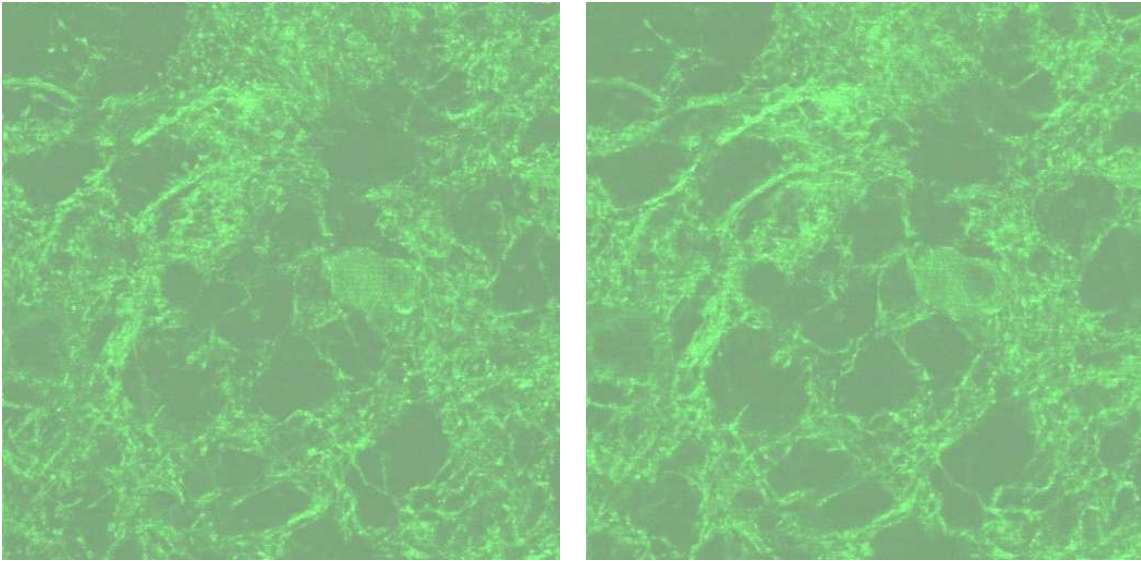


**Fig. 23. Sequential confocal slices of GFP stained mouse brain at 60X.**

Placing each of the slices along an axis, we are able to create our volumetric data set and extract an isosurface representation of the data (Fig. 24). Modifications to the Illumination Subsystem could ideally allow us to gather high-resolution GFP images using the KESM. High-resolution images at a magnification of 40X would allow us to reconstruct the network of interneurons in the mouse cortex.



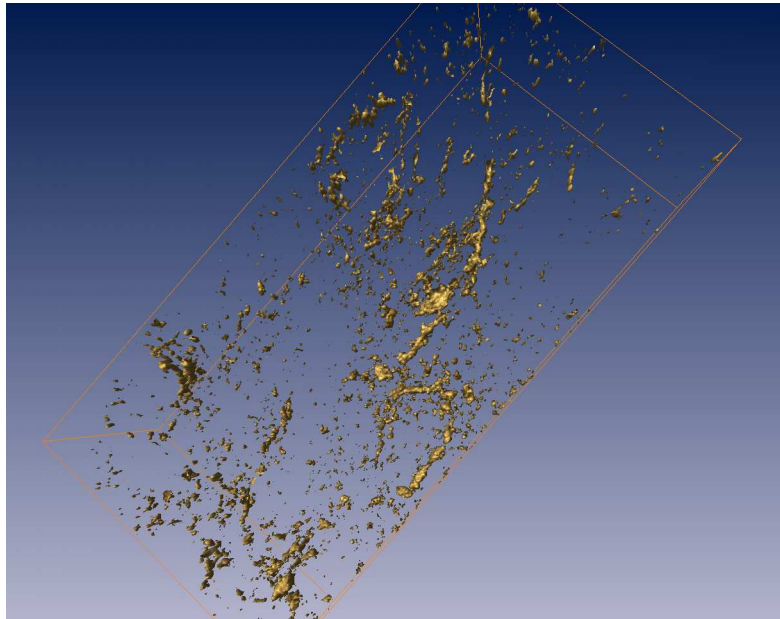


**Fig. 24. Isosurface reconstruction of processes from confocal scans.**

## **APPENDIX B**

### **KESM USER INTERFACE [27]**

The Knife-Edge Scanning Microscope (KESM) integrates several different sophisticated components. The interactions among these components are complex and must be aligned and executed properly to maintain proper registration in the collected tissue data. The need arises quickly for a user interface to hide many of these complicated details.

#### **B.1. Goals**

The KESM User Interface was designed to accomplish four goals.

##### **B.1.1. Ease of Use**

The KESM is a complex system composed of many unique and custom-designed instruments. The interface must allow the user easy and confident control. This is accomplished by using a graphical event driven interface. The user enters data via the keyboard and moves through the interface by clicking buttons. This interface minimizes the number of essential inputs. Any parameter that can be calculated from other data that has been previously determined and stored by the interface does not require user input.

### **B.1.2. Optimize Safety**

Improper use of the KESM equipment can result in bodily harm. To minimize safety risks, a majority of the KESM is computer controlled via the interface. However, other equipment cannot be computer controlled directly and must be controlled physically by the user. Using visual aides, the interface guides the user through the correct procedures to control such equipment (at the correct time).

### **B.1.3. Ensure Security**

Only authorized users are allowed to operate the KESM. A user must have both a login and password to the computer running the interface software, and then must have a login and password to start the interface. Once in the interface system, users may access only their personal experiment data and are restricted to performing tasks for which they are cleared.

### **B.1.4. Minimize Equipment Damage**

A majority of the KESM components are one-of-a-kind and custom built for this project. Because of this, damage to the equipment is both costly and time- consuming to repair. The user interface aims to minimize the chance for equipment damage to several parts of the KESM unit.

The KESM uses an air bearing stage to move the specimen under the stationary collimator assemble that holds the diamond knife and microscope objective. The exacting design of the collimator and specimen tank combined with the range of motion

of the precision stage can easily damage equipment if an improper stage command is given. Damage can occur to the diamond knife, to the collimator assembly, or to the stage itself.

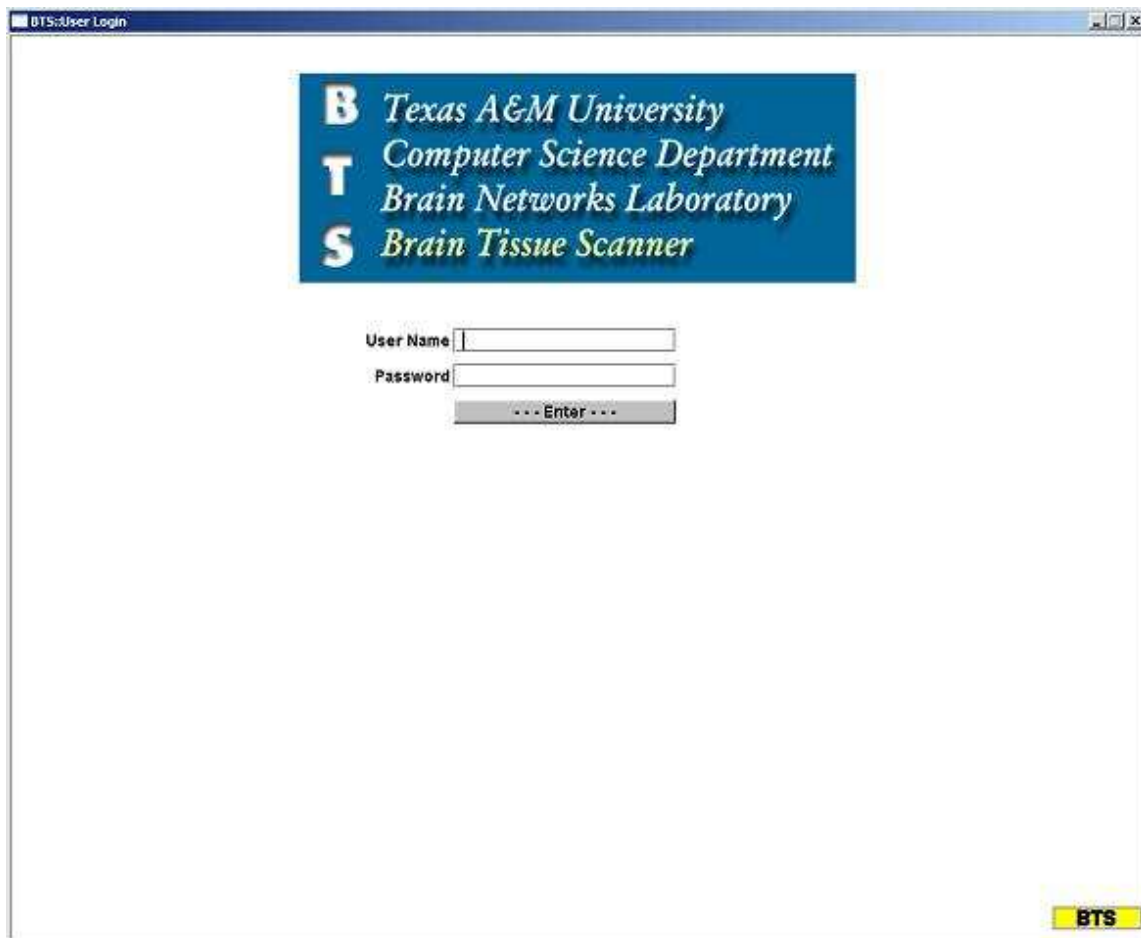
The interface uses three methods to minimize movement damage. First, all stage movements are computer controlled by the interface. No manual stage control is allowed. Second, the interface stores a specimen profile for each specimen that maps the topography of that particular tissue block. Stage movement commands are checked against this profile to ensure that the knife will only section tissue of an acceptable depth and width. Finally, a profile of the specimen tank is stored; as before, the interface checks all stage movement commands against this profile to ensure that the stage does not move in such a way that the walls of the specimen tank or the specimen ring could collide with the collimator assembly or the diamond knife.

Other damage may occur to the stage or stage controller even if stage movement stays within the specified profile. The stage and the stage controller (U500) may become damaged if the input air pressure is not within a desired range. The interface monitors an air pressure sensor and can shut down the stage if the pressure is not correct.

The interface also monitors the audio emissions of the KESM and will shut down the stage if it is emitting sounds outside the norm (such as a loud squealing).

## B.2. Interface Modules

### B.2.1. Login



The screenshot shows a window titled "BTS:User Login". Inside the window, there is a blue rectangular box containing the following text:

**B** *Texas A&M University*  
**T** *Computer Science Department*  
**S** *Brain Networks Laboratory*  
*Brain Tissue Scanner*

Below this box, there are two input fields: "User Name" and "Password". Below the "Password" field is a button labeled "... Enter ...". In the bottom right corner of the window, there is a small yellow button labeled "BTS".

Fig. 25. Login Module.

This module simply allows the user to enter their user name and password and attempt to login to the interface.

### B.2.2. Main Menu

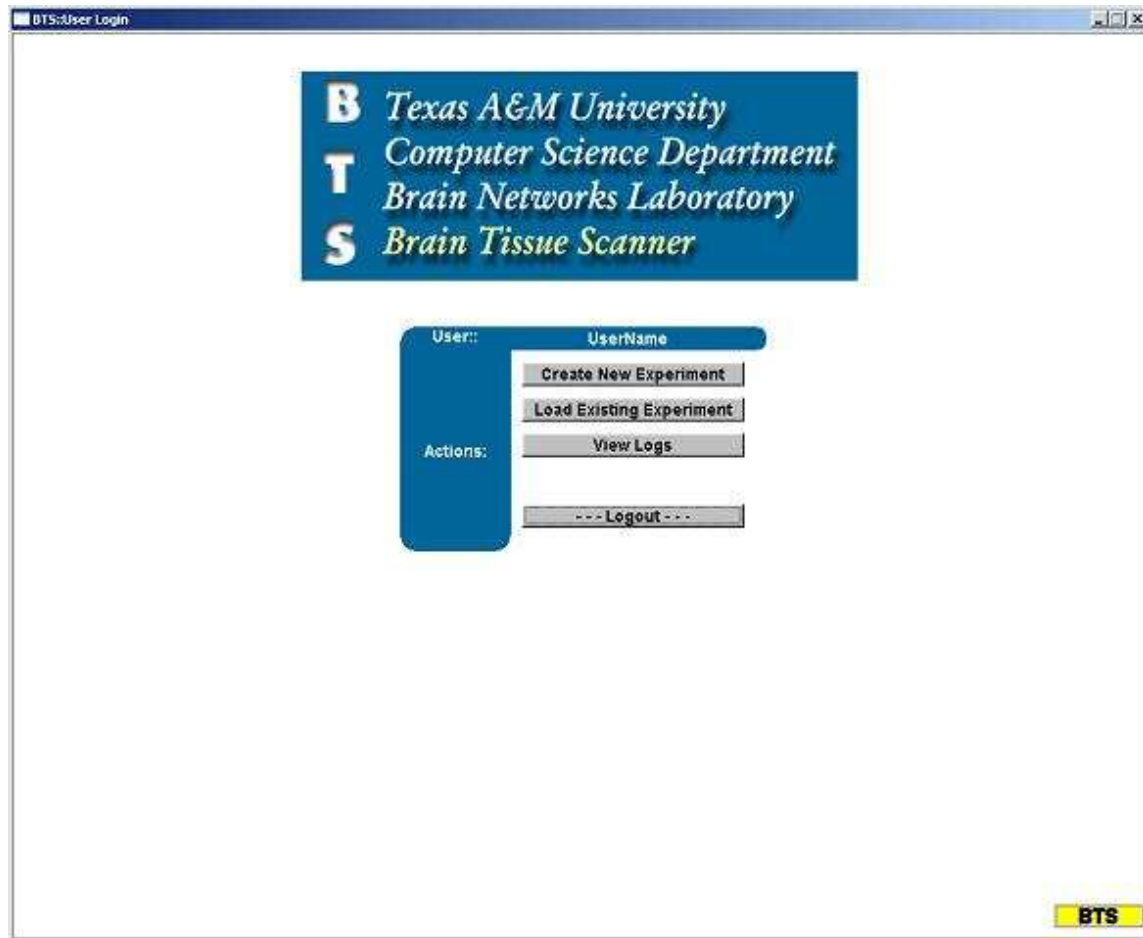


Fig. 26. Main Menu Module.

After logging in, the user sees a display of the main menu. This module allows the user to create of a new experiment, resume an old experiment, view logs and, in the case of system administrators, to access special software used to align the KESM.

### B.2.3. Experiment Parameters

The screenshot shows a software interface for setting experiment parameters. The window is titled "BTS:User Login" and contains the following sections:

- Specimen Source:**
  - Institution:
  - Laboratory:
  - Individual:
  - Date Received:
- Specimen Mounting:**
  - Embedding Material:
  - Mount Type:
    - Type I
    - Type II
    - Type III
- Specimen Data:**
  - Tissue:
  - Block ID:
  - Stain:
- Block Dimensions (mm):**
  - Length(X):
  - Width(Y):
  - Depth(Z):
- Tissue Sectioning:**
  - Coronal
  - Horizontal
  - Sagittal
- Stair-Step Cutting Strokes (mm):**
  - Section Depth:
  - Sections/Plank:
  - Section Width:
  - Max # Planks Deep:
  - Cutting Speed (mm/sec):
- Optical Specs:**
  - Objective:
    - 2x (air)
    - 4x (air)
    - 10x (water immersion)
    - 40x (water immersion)
  - Laser:
    - 473 nm (blue)
    - 488 nm (blue)
    - 532 nm (green)

At the bottom of the window, there are three buttons: "Return to Main Menu", "Accept", and "BTS".

Fig. 27. Experiment Parameters Module.

This module allows the user to input new experiment parameters or to modify existing experiment parameters before starting the sectioning process. The experiment parameters fall into 5 classes: specimen information, specimen block information, sectioning parameters, camera specification, and laser specification.

### B.2.4. Startup Procedure

The startup procedure module guides the user through the correct procedure to initialize the KESM safely. This is done via text descriptions and images depicting the procedure. The interface also initializes the stage and monitoring software (such as air pressure and acoustic monitoring).

### B.2.5. Sectioning & Image Capture

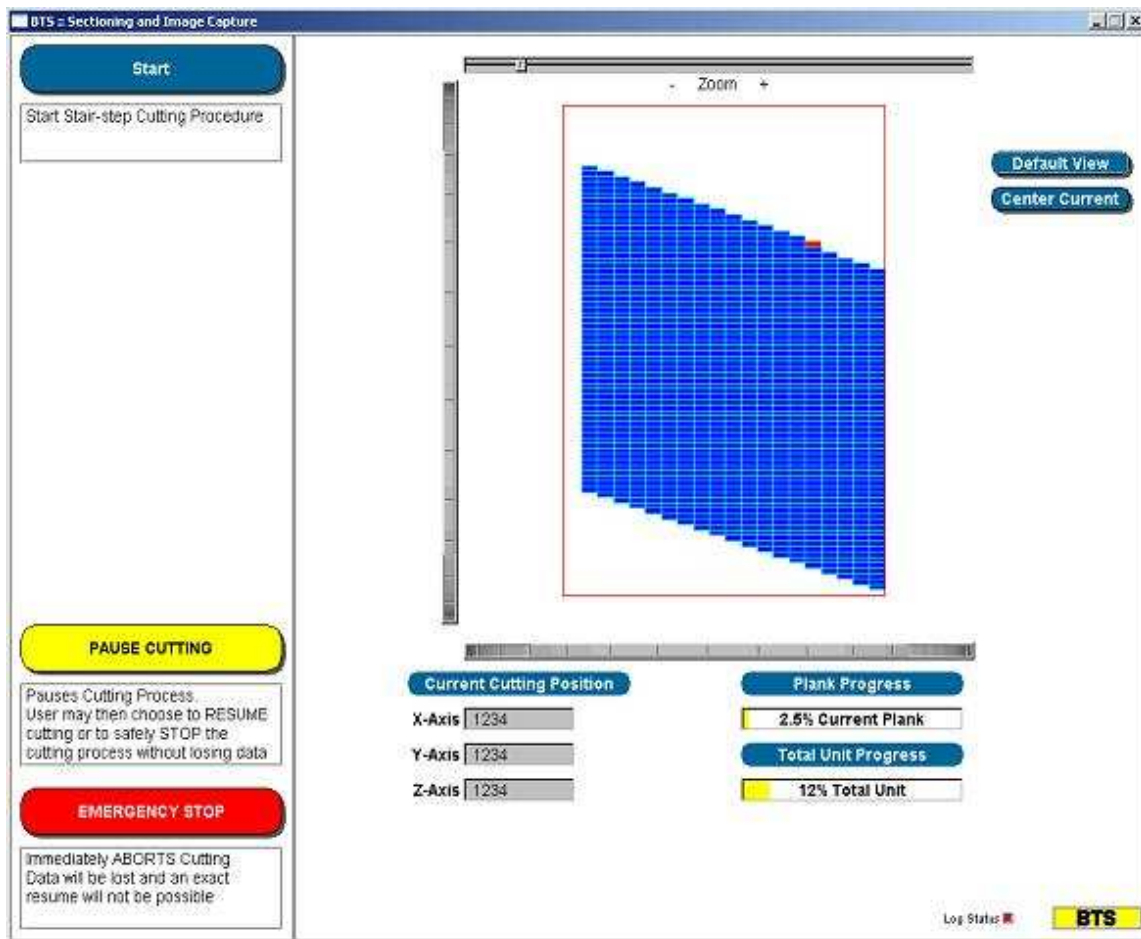


Fig. 28. Sectioning and Image Capture module.



The sectioning and image capture module allows the user to start, stop, and monitor the sectioning and image-capture process. The user may pause the process temporarily and later resume the process, or the user may execute an emergency stop if needed. The interface displays a graphical depiction of the sectioning process and displays percentage complete and stage coordinates.

### B.3. Flow of Control

The flow of control between the modules is basically linear with only a few loops back to other modules.

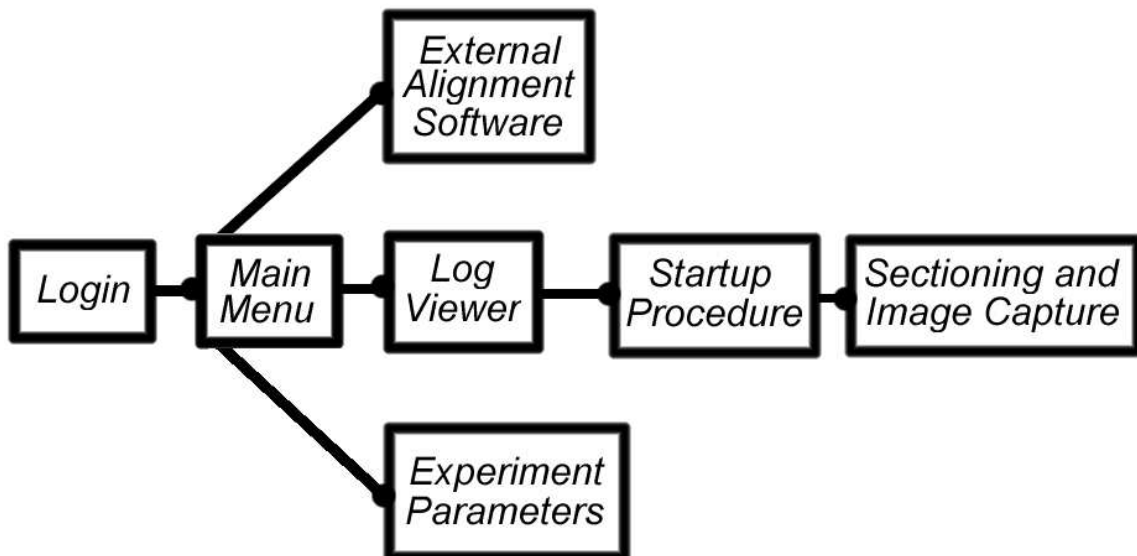


Fig. 29. Module Flow of Control diagram.

#### B.4. Module/Database Interaction

User interface modules interact with specific tables in the KESM database. The mold containing the “potted” specimen sits within the specimen tank.

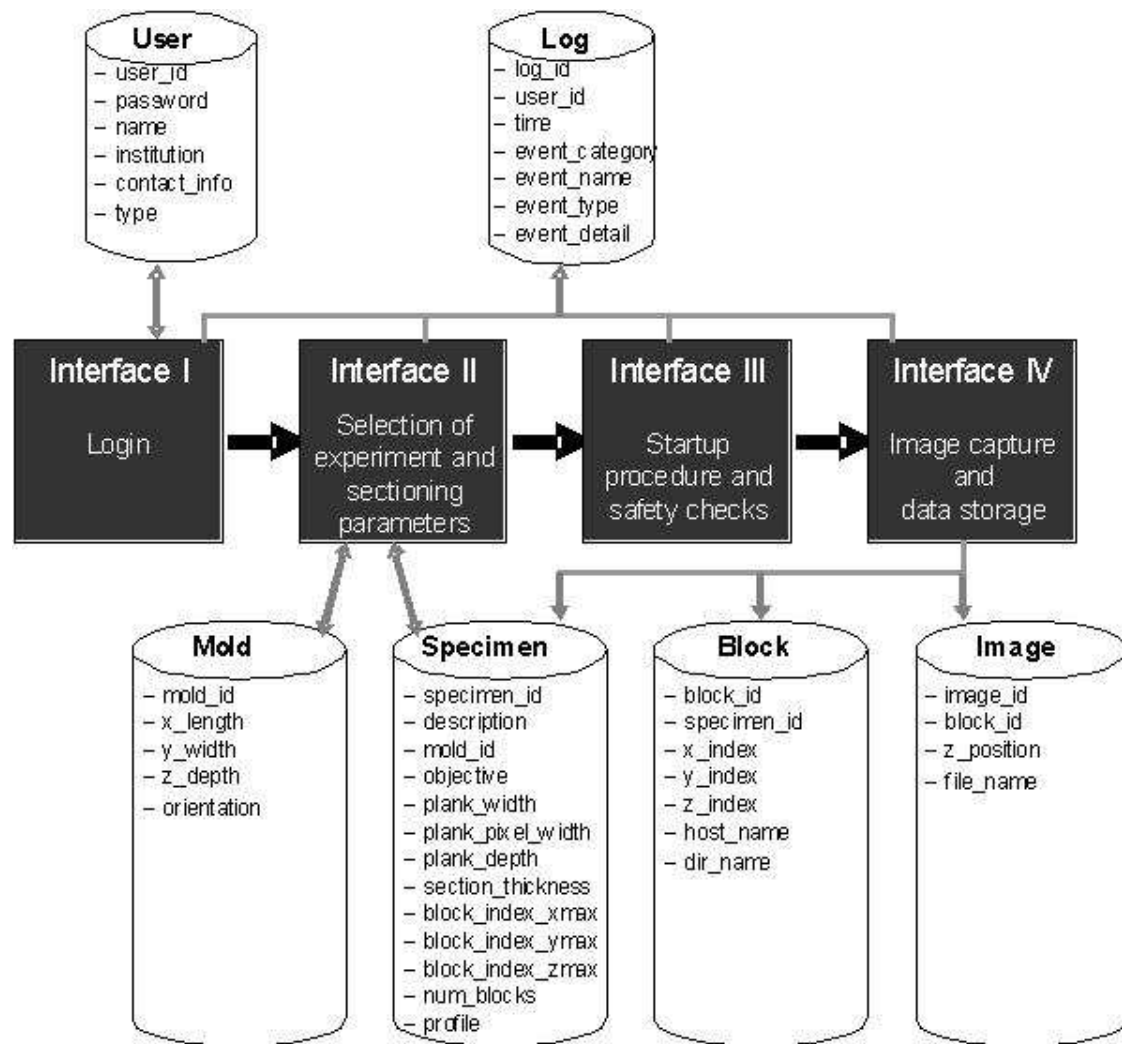


Fig. 30. Interface Module / Database Interactions [27].

## VITA

David Mayerich received a B.S. in Computer Science from Southwestern Oklahoma State University in Weatherford, Oklahoma in August 2000. Since Fall of 2000 he has been working towards his M.S. in Computer Science at Texas A&M University.

He can be contacted by e-mail at [mayerichd@quantumkingdom.com](mailto:mayerichd@quantumkingdom.com) or at the following address:

3667 Wellborn Rd.

Bryan, TX 77801